Postrift stress field inversion in the Potiguar Basin, Brazil – Implications for petroleum systems and evolution of the equatorial margin of South America

Bezerra, Francisco H.; de Castro, David L.; Maia, Rubson P.; Sousa, Maria O.L.; Moura-Lima, Elissandra N.; Rossetti, Dilce F.; Bertotti, Giovanni; Souza, Zorano S.; Nogueira, Francisco C.C.

DOI
10.1016/j.marpetgeo.2019.08.001

Publication date
2020

Document Version
Accepted author manuscript

Published in
Marine and Petroleum Geology

Citation (APA)
Bezerra, F. H., de Castro, D. L., Maia, R. P., Sousa, M. O. L., Moura-Lima, E. N., Rossetti, D. F., Bertotti, G., Souza, Z. S., & Nogueira, F. C. C. (2020). Postrift stress field inversion in the Potiguar Basin, Brazil – Implications for petroleum systems and evolution of the equatorial margin of South America. *Marine and Petroleum Geology*, *111*, 88-104. https://doi.org/10.1016/j.marpetgeo.2019.08.001

Postrift stress field inversion in the Potiguar Basin, Brazil – implications for petroleum systems and evolution of the equatorial margin of South America

Francisco H. Bezerra[1], David L de Castro[1], Rubson P. Maia[2], Maria O. L. Sousa[1], Elissandra N. Moura-Lima[3], Dilce F. Rossetti[4], Giovanni Bertotti[5], Zorano S. Souza[1], Francisco C. C. Nogueira[6]

[1]Departamento de Geologia, Universidade Federal do Rio Grande do Norte, Natal, Brazil

[2]Departamento de Geografia, Universidade Federal do Ceará, Fortaleza, Brazil

[3]Unidade Acadêmica de Mineração e Geologia, Universidade Federal de Campina Grande, Campina Grande, Brazil

[4]Divisão de Sensoriamento Remoto, Instituto Nacional de Pesquisas Espaciais, Brazil

[5]Faculty of Civil Engineering and Geosciences, Delft University of Technology, The Netherlands,

[6]Centro de Ciências e Tecnologia, Universidade Federal de Campina Grande, Campina Grande, Brazil

Correspondence to: Francisco Hilario Bezerra, bezerrafh@geologia.ufrn.br

Abstract

Rifting and related normal stress regime in the equatorial continental margin of Brazil ceased during the Late Cretaceous, when the stress regimes in eastern South America and West Africa changed to induce strike-slip or reverse motion. In this study, we explore the postrift tectonic, geomorphic, magmatic, and sedimentary responses to stress changes using the Potiguar Basin, the easternmost basin in the equatorial margin of Brazil, as a case study. We use field and topographic data, 2D seismic reflection lines, vertical electric soundings, and geochronological and borehole data to constrain the stress evolution of the Potiguar Basin from the Late Cretaceous to the Quaternary, discussing the role of basin inversion on sedimentation and landforms. Our results indicate the presence of two strike-slip stress regimes after rifting. The first stress field (SF1) occurred from Late Cretaceous to the middle Miocene and consisted of a N-S-oriented maximum subhorizontal compression and an E-W-oriented extension. The second stress field (SF2) took place from the middle Miocene to the present day and included subhorizontal E-W to NW-SE compression combined with N-S and NE-SW subhorizontal extension. Emplacement of volcanic rocks occurred along transtensional faults, with a principal peak during SF1 at 20-30 Ma and a subordinate peak during SF2 at 5-10 Ma. In response to shortening during SF2, a 70-km-long and 50-km-wide dome formed, where marine Miocene strata were uplifted to ~250 m asl. This uplift induced the displacement of alluvial channels away from the dome. Anticlines formed by transpression along the main NE-SW-striking faults during both SF1 and ST2 acted as traps in the petroleum system. Similar shifts and stress field inversions documented in other areas of the Brazilian continental margin are consistent with the Neogene rise of the

Andes and may have implications for reconstructing the tectonic history of the Equatorial Atlantic margin of South America.

Keywords: Neotectonics, basin inversion, stress field, equatorial margin, tectonic uplift

1. Introduction

The postrift evolution of continental margins is, in theory, characterized by thermal subsidence related to lithospheric cooling and associated thickening (McKenzie, 1978). The postrift stage can evolve into a passive margin, which was initially viewed as being marked by tectonic quiescence. However, many passive margins worldwide have been subjected to inversion, such as in eastern Canada (Withjack et al., 1995), the North Sea (Doré et al., 2008), the western Ghats in India (Gunnel and Fleitout, 2000), Rockall Trough off Great Britain (Boldreed and Anderson, 1993), southeastern Brazil (Cobbold et al., 2001), and West Africa (Hudec and Jackson, 2002).

The processes that drive the postrift evolution of a passive margin remains elusive, and two main points are still open to debate. First, the first-order stress fields on most present-day continental margins are well established, but they are not necessarily the same as those that existed during the early postrift stage, which are still poorly documented (e.g., Dyksterhuis et al., 2005; Sippel et al., 2009). Second, there are several examples of rift-related basin inversion on passive margins (e.g., Müller et al., 2014), but geophysical data (e.g., seismic reflection sections) have been unable to unravel most postrift structures, which are either very shallow or below seismic resolution.

Most basins on the conjugate margins of eastern South America and West Africa are considered to be examples of the ‘passive’ extensional basin type described by McKenzie (1978). On the equatorial margins of these continents, rifting has evolved from wrench tectonics in the Late Jurassic to the Early Cretaceous to a passive margin stage that began in the Late Cretaceous (e.g., Moulin et al., 2010). After continental rifting, these basins underwent tectonic quiescence, during which the tectonics were presumably controlled by thermal subsidence (Matos, 1992; Maurin and Guiraud, 1993). However, flexural effects on passive margins offset by oceanic fracture zones might not follow the classic thermal subsidence model described by McKenzie (1978), and later critically assessed by Braun et al. (2013).

At the basin scale, changes in plate motions on the equatorial margins of South America and Africa have changed the stress field and affected the fault geometries and kinematics as much as the resulting basin stratigraphy (Fairhead and Binks, 1991). Nonetheless, many studies have failed to explain the evolution of these conjugate margins after continental breakup. Despite mounting evidence of basin inversion (Cobbold et al., 2001; Marques et al., 2014; Nogueira et al., 2015) as well as folding and uplifting of Neogene and Quaternary coastal sediments (e.g., Rossetti et al., 2013; Gandini et al., 2014), linking the normal faulting stress regime during the breakup of Pangea to the present-day intraplate strike-slip to reverse stress regime is still a challenge. In addition, several consequences of this stress field inversion such as topographic and sedimentary changes have not been fully assessed.

The paleostress evolution of the equatorial margin is not well known, especially after rifting ceased in the Cretaceous. Predicting stress fields along sheared continental margins is difficult because little is known about the mechanical interaction between the two plates. For example, the present-day intraplate stress field in South America is controlled by its collision with the Nazca Plate and the rise of the Andes (Garcione et al., 2008; Marques et al., 2014; Nogueira et al., 2015; Assumpção et al., 2016). However, to what extent the spatial and temporal variations of the upper-crustal deformation in the central Andes are related to shifts in the intraplate stress field of South America remains an unsolved question. Therefore, understanding the controlling factors of stress evolution during the postrift period is important for unravelling the geological evolution of the Atlantic margin.

This work aims to understand the evolution of the stress fields between the normal fault stress regime during the breakup of Pangea and the present-day intraplate strike-slip stress regime in equatorial South America. The main objectives of this study are (1) to determine the evolution of the stress field during the postrift period; (2) to identify the timing of tectonic inversion; (3) to investigate the effects of inversion on Neogene-Quaternary sedimentation and landforms; (4) to investigate the implications of stress field inversion in the petroleum geology system of the Potiguar Basin; and (5) to assess the importance of the Potiguar Basin to better understanding the evolution of Equatorial Brazil's offshore region.

We selected the Potiguar Basin in the equatorial margin of Brazil as a case study for several reasons. First, it is composed of a long stratigraphic record comprising sedimentary units that span from the Neocomian (~138 Ma) to the Late Quaternary in an aborted rift located on the passive continental margin of northeastern Brazil (e.g., Matos, 1992; de Castro et al., 2012). Second, it is located in a region that was the last segment of the South American Plate to breakup from the African Plate (Azevedo, 1991; Matos, 1992). A significant portion of the seismicity in South America is also concentrated in this region, where the highest ground peak acceleration in intraplate South America is recorded (Shedlock and Tanner, 1999). Finally, it contains a variety of present-day stress markers such as focal mechanisms, breakouts, and image logs (e.g., Ferreira et al., 2008; Bezerra et al., 2011; Reis et al., 2013), so it is a good area to correlate the paleo- and present-day stress fields (Fig. 1). The multidisciplinary investigation carried out in the Potiguar Basin allowed us to better understand the postrift evolution of Equatorial Brazil's offshore region, improving the current knowledge about the opening of the Atlantic and related plate reconstructions.

2. Tectonic and stratigraphic settings

2.1. Rift-to-drift evolution of the Potiguar Basin

The Potiguar Basin is located in the eastern part of the Brazilian equatorial margin. This basin is an aborted rift located on the narrowest continental margin of Brazil (Fig. 1A), and is limited to the south and west by Archean and Proterozoic crystalline basement, respectively (Van Schmus et al., 1995; Souza et al., 2013, 2016). The Potiguar Basin is composed of a main NE-SW-oriented central graben that is ~6 km deep and ~50 km wide, bounded by two horsts (Fig. 2). The central graben formed at 130 Ma, when ductile Precambrian shear zones were reactivated during continental rifting (Matos, 1992; De Castro et al., 2012). Rifting evolved from NW-SE-oriented extension in the Neocomian to E-W-oriented extension in the Barremian (Matos, 1992). Most of the rift faults in the Potiguar Basin strike NE-SW, whereas the transfer faults that accommodate displacements between different rift segments strike NW-SE (Bertani et al., 1990; De Castro and Bezerra, 2015). Postrift reactivation of these faults propagated them into Late Cretaceous to Cenozoic strata, although with lower slip rates (Bezerra and Vita-Finzi, 2000; Nogueira et al., 2010).

The sedimentary filling of the Potiguar Basin consists of three major depositional sequences: rift, transitional, and postrift. The first two sequences are buried and cannot be directly investigated in the field (Fig. 2). However, the postrift sequence crops out in the basin and contains stratigraphic markers that can be used to constrain the ages of the paleostress fields.

The lithologies, locations, and ages of four postrift sedimentary and a volcanic unit are well constrained in the Potiguar Basin. The Açu and Jandaíra Formations record the first phase of the opening of the South Atlantic, which occurred in the Late Cretaceous. The Açu Formation contains siliciclastic alluvial deposits (Fig. 2) deposited from the Albian (110 Ma) to the Cenomanian (94 Ma), whereas the Jandaíra Formation records carbonates that formed in tidal to shallow shelf environments from the Turonian (93 Ma) to the Campanian (80 Ma) (Pessoa Neto et al., 2007). These units cap transitional and rift sequences in the central graben but lie directly over the crystalline basement in the eastern and western horsts (Fig. 2) (Sousa Filho et al., 2000). Soares et al. (2012) and Alves et al. (2017) have shown these "transitional' sequences to be associated with continental breakup.

The Barreiras Formation caps the Late Cretaceous units and consists of several siliciclastic lithologies deposited in various marine-influenced transitional environments (Rossetti et al., 2013). This unit is present in several sedimentary basins along the Brazilian coast and is particularly well exposed in numerous coastal cliffs up to ~40 m high. The age of the Barreiras Formation is based on its stratigraphic relationships with other Oligo-Miocene sedimentary units in the western part of the Brazilian equatorial margin (e.g., Rossetti, 2004). In addition, pollen data are consistent with an early-middle Miocene age for this unit (e.g., Arai et al., 1988; Arai, 1997). This age was confirmed by Ar/Ar and U/Th-He chronology, which constrained the depositional ages to between 23 Ma and 17 Ma (Lima, 2008; Rossetti et al., 2013).

The Quaternary sediments are mostly composed of sandy to gravelly alluvial deposits with optically stimulated luminescence ages ranging from 400 ka to 0.4 ka (Moura-Lima et al., 2011). These deposits occur as alluvial sediments along recent valleys and paleovalleys (Moura-Lima et al., 2011) and as colluvial sediments along fault scarps (Gurgel et al., 2013).

The Cenozoic volcanic and hypabyssal rocks are related to the Macau volcanism (Fig. 2). They cut across the Late Cretaceous units, the Barreiras Formation, and the crystalline basement. In the present study, we focused on the magmatic units that exhibit wide expression in the Potiguar Basin, which includes both alkaline and tholeithic basalts (Sial, 1976; Almeida et al., 1988; Souza et al., 2003, 2005) that have K-Ar and ^{40}Ar-^{39}Ar ages ranging from 47 to 7.4 Ma with a prominent peak at 30-10 Ma and minor peaks at 50-40, 40-30 and 10-0 Ma (Tab. 1 and Fig. 3). There are also volcanic bodies in the Potiguar Basin with older ages at 93 Ma and 70-50 Ma but these are limited to small volcanic bodies (Souza et al., 2004), lacking a wider expression proving they influenced the deformation pattern of the sedimentary basin. Based on the chemistry of inclusions in these units, Sial (1976, 1977) and Rivalenti et al. (2000) estimated that these basaltic magmas originated at pressures of 19 to 27 kbar or depths of approximately 60-90 km. There are several interpretations for the origin of these volcanic rocks, including: (1) the surface track of the Fernando de Noronha plume (Fodor et al., 1998; Rivalenti et al., 2000); (2) the influence of an oceanic fracture zone (Almeida et al., 1988); (3) the result of either an internal readjustment within the South American plate during its westward migration, or the pressure release of arched zones that formed in the Cretaceous during the opening of the South Atlantic Ocean (Sial, 1976; Carneiro et al., 1988); or (4) the manifestation of the upwelling flow in an edge-driven convection mode (Knesel et al., 2011). Despite its controversial origin, these workers agree that the magma from these intrusions ascended from the uppermost portion of the upper mantle to the very shallow continental crust along deep fault systems.

2.2. Present-day stress field and seismicity of the eastern equatorial margin

The present-day stress field in the Potiguar Basin and its crystalline basement is well constrained by three types of stress indicators: focal mechanisms, borehole breakouts, and image logs. In general, strike-slip faulting predominates, but normal and reverse faulting also occur. The focal mechanisms of events at depths between 1 and 12 km indicate that the maximum horizontal compression (S_{Hmax}) trends E-W in the eastern part of the basin, shifts to NW-SE in the central and western parts of the basin, and then shifts again to E-W between the Potiguar and Paraiba basins (e.g., Ferreira et al., 1998, 2008, Bezerra et al., 2011) (Fig. 1B). The inversion of focal mechanisms in the eastern and western parts of the region indicates a strike-slip faulting regime with the maximum compressive stress (σ_1) subhorizontal and parallel to the coastline, the minimum stress (σ_3) orthogonal to the coastline, and a subvertical intermediate compressive stress (σ_2). The stress axis σ_1 shift to ENE-WSW-oriented and σ_3 NNE-SSW-oriented away from the Potiguar Basin in the western and southern parts of the study area (Lima Neto et al., 2014; Oliveira et al., 2015) (Fig. 1B). The borehole breakout orientations are consistent with those observed in the focal mechanisms. In the central part of the Potiguar Basin, breakouts indicate a NW-SE-oriented S_{Hmax}, although a scattered pattern occurs offshore in the continental platform (Lima et al., 1997) (Fig. 1B). The image logs are also consistent with both stress indicators described above. However, the image logs indicate that a normal stress regime is present in the central part of the basin at depths of 0-2.5 km. These stresses change to a strike-slip/normal regime below 2.5 km, which is consistent with the focal mechanisms recorded in the crystalline basement from 1 to 9 km. This stress decoupling has been considered to be an indication of inversion and bending of the upper layers in the

Potiguar Basin (Reis et al., 2013). All of these stress indicators consistently indicate a maximum horizontal compression roughly parallel to the coastline, which has been interpreted as the effect of the density contrast between the continental and oceanic crust (Assumpção, 1992; Ferreira et al., 1998; Oliveira et al., 2015).

Strain data from a permanent GPS network have also been reported for the Potiguar Basin and adjacent regions (Marotta et al., 2015). The velocity direction trends predominantly west and north with maximum rates of 4.0 ± 1.5 mm/year and 4.1 ± 0.5 mm/year for the x and y components, respectively. The largest contractional strain was -0.072838 x 10^{-6} ± 2.32 x 10^{-10}/year and was oriented NW-SE in the Potiguar Basin, and the maximum extensional strain was 0.109552 x 10^{-6} ± 3.65 x 10^{-10}/year and was oriented NE-SW, also in the Potiguar Basin. These results indicate that the greatest strain and variation in velocity are located in the crystalline basement near the Potiguar Basin and also that the shortening/compression direction is consistent with the maximum horizontal stress indicated by the three stress markers presented above (Marotta et al., 2015).

Historical and instrumental seismicity data show that the border of the Potiguar Basin is seismically active. These data also indicate that this basin exhibits a relatively high level of seismicity compared to other 'passive' margin basins in eastern South America. The Potiguar Basin has been affected by sequences of earthquakes that can last 10 years or more and have body-wave (m_b) magnitudes up to 5.2 (Bezerra et al., 2007; Assumpção et al., 2014). The seismicity and the location where the stress has been released affect the crystalline basement around and underneath the Potiguar Basin at depths from 1 to 12 km

(Takeya et al., 1989; Ferreira et al., 1998; do Nascimento et al., 2004; Lima Neto et al., 2013, 2014; Oliveira et al., 2015).

3. Methods

3.1. Paleostress analysis

Paleostress tensors were reconstructed based on a detailed field study and the analysis of fault populations. The field investigation included 271 outcrops that were grouped into 30 sites, where slip data for 1127 faults were measured. In a few locations, joint-stylolite geometries and their cross-cutting relationships were analyzed using drone images with 1 cm pixel sizes to constrain the fault-slip data. The fault-slip data consisted of the orientations of fault planes and related striations, slip senses, and the quality of the kinematic indicators. A variety of kinematic indicators were used to determine the slip senses of faults, including mineral steps, tension gashes, Riedel shears, conjugate shear joints, and overgrowths of differently oriented fibers on the same fault (Hancock, 1985; Petit, 1987; Angelier, 1994). In addition, stylolites were utilized as paleostress indicators when their occurrence allowed a statistical analysis.

The following criteria guided the investigation of the relative chronology of the stress markers in the field: (a) cross-cutting relationships between faults and joints; (b) overprinting relationships between striae on a fault plane; (c) the ages of the stratigraphic units affected by faults and joints; (d) the persistence and consistency of kinematic indicators along a fault plane; and (e) splitting of inhomogeneous fault-slip data from kinematically compatible sets. We applied all of these criteria to identify successive tectonic events and their related stress fields. Where sparse data, we analyzed outcrops separately but merged the data from neighboring outcrops in similar stratigraphic units that were not separated by fault zones. We then determined the stress tensors by combining the stratigraphic information with the relative order of the fault–slip data sets. We only used the automatic separation of the fault-slip data to cross-check the results derived from the criteria presented above.

Stress tensors were determined using several steps. Each reduced stress tensor comprises the directions and plunges of the principal stress axes ($\sigma_1 \geq \sigma_2 \geq \sigma_3$) and the stress ratio R = (σ_2-σ_3)/(σ_1-σ_3) (Angelier, 1979). We used the direct inversion method (Angelier, 1990, 1994) based on Bott's principle (Bott, 1959), which we processed in the Tectonics FP package (Otner et al., 2002). In addition, we imposed a quality standard for the fault-slip data. For example, faults with striae deviating by more than 10° from the fault plane were disregarded, and only corrected fault sets were used to calculate the orientations of the principal axes.

3.2. Seismic, geoelectric and topographic investigations

Seismic, geoelectric and borehole data were utilized to investigate the architecture of the Potiguar Basin and the postrift tectono-sedimentary fill in the central part of the basin. The data included three previously stacked and migrated 2D seismic sections and three exploratory wells from the Brazilian Petroleum Agency (ANP) database. In addition, 30 vertical electric soundings (VESs) were performed along a 55 km profile near one seismic line and oriented roughly perpendicular to the rift faults. We used the VESs to define geoelectric layers and the internal geometry of the uppermost part of the basin, where the seismic lines have poor resolution. The soundings were spaced 2.0 km apart, and all of the measurements were taken using Schlumberger's electrode array with current electrode half-spacings (AB/2) ranging from 1.5 m to 600 m. We used a Tectrol resistivity meter with a maximum power of 500 W, which was able to provide the apparent resistivity with high accuracy for estimated investigation depths of 250-300 m. Estimates of the resistivity and thickness were calculated from the VES data using the IPI2Win software developed by Bobachev (2003). Interactions using this code were carried out automatically and interactively until the calculated model satisfied a minimum difference between the measured and calculated data.

The results are presented in a geoelectric pseudo-section derived from 1-D inversions of each of the 30 VESs, which were applied separately to obtain the resistivity distribution in the shallow subsurface (Fig. 4). Seismic and well information were used to constrain the 1-D inversion and interpret the geoelectric pseudo-section. The root-median-square misfits between the observed and calculated geoelectric curves (RMS errors in Fig. 4) are in the range of 0.25 - 12.7%.

4. Results

4.1. Postrift paleostress fields

Two paleostress fields were identified based on the criteria outlined in Section 3. We list the site locations, amount of data, and stress tensors for each stress field in Table 2. Each stress fields are presented below with the general stress parameters, and the analysis of the deformation structures and their significance.

Stress field 1 (SF1) was identified in both the siliciclastic units of the Açu Formation and the carbonates of the Jandaíra Formation. Most sites revealed polyphase deformation reaching two stress fields. A total of 22 stress tensors represent SF1, 14 of which are strike-slip tensors, 2 are normal tensors, and 6 are reverse stress tensors. The stress tensors indicate a subhorizontal N-S-oriented σ_1 and a subhorizontal E-W-oriented σ_3 (Fig. 5, Table 2). SF1 is also marked by a set of N-S-striking mode I joints and orthogonal E-W-striking vertical stylolites. The maximum horizontal compression (σ_1) is consistently oriented N-S with a ~10° variation in azimuth and a ~5° variation in plunge. Generally, σ_2 is subvertical, and σ_3 is generally subhorizontal with an E-W-trend, but these two axes shift position at several sites (Fig. 5). The mean concentration of stress tensors indicates the following: 357/15 σ_1, 268/98 σ_2, and 087/60 σ_3 (Fig. 5). The stress ratios (R) for SF1 range from 0.8234 to 0.2185. The changes from the main strike-slip regime to the local normal and reverse regimes are due to shifts between σ_2 and σ_3 or between σ_1 and σ_2. Faults of SF1 are pervasive in the basin, as attested by remote sensing and field data from current and previous studies (Bezerra et al., 2009, 2014).

SF1 was followed by a second stress field (SF2). Where a relative chronology could be established, the faults and joints of SF2 systematically postdate those of SF1. Less than 50% of the faults from either SF1 or the rift phase were reactivated during SF2. We obtained 21 stress tensors (Fig. 6, Table 2), of which 15 indicate a strike-slip regime, 1 indicates a normal fault regime, and 5 indicate a reverse fault regime. These stress tensors also indicate partitioning between strike-slip and normal faulting. SF2 shows a subhorizontal E-W-trending σ_1, a subvertical σ_2, and a subhorizontal N-S-trending σ_3 in the eastern part of the basin. However, σ_1 and σ_3 rotate clockwise in the western part of the basin, where σ1 trends WNW-ESE, and σ_3 trends NNE-SSW at four sites. The mean SF2 of the stress tensors yielded 267/18 σ_1, 270/84 σ_2, and 023/63 σ_3 (Fig. 6) with R ranging from 0.9928 to 0.0481 (Table 2). The variation in R is larger than that observed in SF1. Approximately 50% of the major faults of SF2 are the same as those of SF1, suggesting that the reactivation of pre-existing faults was the mode of failure during SF2 at several sites.

The differences in the directions of the maximum compression (σ_1) for the strike-slip faults of SF1 (N-S trends) and SF2 (mostly E-W trends) indicate that the paleostress tensors for each stress field can be grouped as a single tectonic episode. However, the permutation between σ_2 and σ_3 and the wide range in R in both stress fields indicate that the relative magnitudes of the principal stress axes vary, although they exhibit the same orientations.

4.2. Major postrift faults and volcanic units

In the postrift period, the major structures of the main graben and horsts in the rift phase were reactivated, and new faults were generated. We focus on the central part of the basin, where the major faults are closely associated with basaltic volcanic units (Fig. 7).

These faults are mainly NW-SE-striking dextral faults and NE-SW-striking sinistral faults.

The location, geometry, and age of the volcanic rocks in the Potiguar Basin and the adjacent basement indicate their relationship to the major faults. Most of the basaltic rocks in the onshore area of the Potiguar Basin form NW-SE-oriented bodies along the NW-SE-striking Afonso Bezerra Fault and other parallel faults (Fig. 7A). Some of the volcanic rocks are deformed by right-lateral fault offsets (Fig. 7B), which indicate magmatic injection mainly during SF1. This is observed on the eastern contact of the Serra Preta basaltic body, which is marked by a right-lateral strike-slip fault of SF1 (numbered 1 in Fig. 7B). Other volcanic bodies, such as the Serra Aguda plug (numbered 2 in Fig. 7B), are intersected by the NW-SE-striking faults. As shown in Table 1, the existing K-Ar ages of the Serra Aguda and the Serra Preta bodies are 24.6±6.0 Ma and 18.0±0.5 to 13.9±2.0 Ma, respectively. These results constrain the end of the SF1 event and the onset of the SF2 event to between 25 Ma and 14-18 Ma.

4.3. Geophysical evidence of tectonic inversion

The analysis of several rift structures is relevant for reconstructing the evolution of the postrift phase. The three seismic lines reveal an internal geometry composed of two main half-grabens that dip to the SE and are separated by a central basement horst (Figs. 8, 9A, B, C). Intracrustal listric normal faults controlled the graben geometry. The border faults and other faults nearby were reactivated by uplifting the most recent layers (RF in Fig. 9A, B, C). A subhorizontal unconformity marks the stratigraphic contact between the synrift and postrift sequences (U in Fig. 9A). Evidence of tectonic inversion is present in the central part of the main graben, where subvertical listric faults exhibit reverse displacements in the rift layers. Each seismic line contains evidence of reverse faulting, although the throws of these fault are much smaller than those of the rift faults (RF in Fig. 9A, B, C).

The main graben observed in the seismic lines (Fig. 9A) coincides with the area of highest topography in the basin, which we defined as the Mel Dome (Figs. 8; distance from 2 to 26 km in Fig. 9A). A section derived from the interpretation of a geoelectric survey along this dome to a depth of 300 m combined with well data reveals details not observed in the seismic lines (Fig. 10). This section combined the results of 1D inversion of the resistivity data from all 30 VESs. Figure 4 displays the individual inversions of VESs 1, 12, 21, and 30, whose geoelectric patterns are characterized by three to six resistivity layers with a large resistivity range (10 to 15500 Ω.m). The upper high-resistivity layer may be caused by dry soil on the surface, which is apparently absent in VES30 (Fig. 4D). VES12 and VES21 are located at the Mel Dome and display a sequence of very high- (<10000 Ω.m) and low- (~10 Ω.m) resistivity layers related to silty and clayey units of the Barreiras Formation. The underlaying low- to medium- (30 to 750 Ω.m) resistivity layers represent the carbonate units of the Jandaíra Formation. The interpreted geoelectric section (Fig. 10) indicates that the highest portion of the Mel Dome is in the half-graben, which is controlled by a border fault (at a distance of 28 km in Fig. 10). We identified a basal layer in the wells that represents the postrift siliciclastic sequence (Açu Formation; yellow layer in Fig. 10). In this area, the carbonate Jandaíra

Formation (blue layer in Fig. 10) and the Miocene siliciclastic Barreiras Formation (brown and green layers in Fig. 10) are thicker in the central part of the dome, suggesting that the postrift sedimentary unit was originally deposited in a topographic depression that was later uplifted by tectonic inversion. The marine Barreiras Formation forms the top of a gently folded dome (the Mel Dome) with elevations ranging from 0 m along the shoreline to at least 200 m in the central part of the dome.

4.4. Surface evidence of tectonic inversion

The Potiguar Basin is marked by tablelands of Cretaceous limestones that dip 2°-3° to the north. These tablelands are interrupted by a fold in the central part of the basin, which corresponds to the Mel Dome. The dome has a NE-oriented elliptical shape and is ~50 km long, ~35 km wide, and 273 m high. We distinguish this dome (Fig. 11) from those related to volcanic activity, which are circular and smaller. The Mel Dome caused the shoreline to advance more than 10 km seaward. This position of the Barreiras Formation constitutes a unique feature of the Brazilian coast.

In the postrift phase of a sedimentary basin, the rivers would be expected to drain towards the centre of the basin due to thermal subsidence. However, the Mel Dome exhibits radial drainage, where the rivers drain away from the central trough in the directions of two valleys: Assu to the east and Mossoró to the west (Fig. 11). Uplift of the Mel Dome stimulated renewed sedimentation to form the Quaternary alluvial deposits. In addition, the traces of the rift faults are oblique to the Assu Valley, but they match the Mossoró

Valley, where they form topographic breaks, indicating that the deformation continued into the Miocene-Quaternary (Fig. 8).

5. Discussion

5.1. Ages of stress fields

The Potiguar Basin has been affected by two nearly orthogonal stress fields since the Campanian. The stress tensors shifted almost orthogonally from SF1 to SF2. Both stress fields exhibit subhorizontal compression oblique to the rift faults. The relationship between the faults and the stress field indicates oblique-slip movements of the major rift faults in both stress fields. Transpression and transtension coexisted during both strike-slip regimes.

Our study is the first to present paleostress evidence for two stress fields during the Late Cretaceous-Cenozoic on the South American equatorial margin. Both stress fields are younger than the rifting, and their ages can be constrained by stratigraphic correlations. Rifting along the equatorial margin of South America started in the Neocomian (ca. 140 Ma) (Matos, 1992; Gasperini et al., 2001) and ceased in the Albian (ca. 110 Ma) (Mascle et al., 1988). This time period represents the maximum age of SF1. In the Potiguar Basin, deformation structures related to SF1 are located in the Açu and Jandaíra formations and in the Miocene Barreiras Formation (23-17 Ma) at a few sites. This indicates a minimum early Miocene age for SF1.

SF1 was followed by SF2, which affected the Miocene and Quaternary sedimentary units. This shift in the stress field occurred from the early to middle Miocene. During SF2, reactivation occurred along the varied geometric style of the SF1 phase. The fault-slip data indicate continuous deformation along faults from the middle Miocene to the present. The shift from SF1 to SF2 also corresponds to the end of the major pulse of the Macau volcanism (Fig. 3) and to the onset of the deposition of the Barreiras Formation (Rossetti et al., 2013).

Mainly during SF1, faults allowed mantle magmas to reach the upper crust and controlled the emplacement of several shallow volcanic and hypabyssal bodies (e.g., dikes, sills, plugs, laccoliths, and lopoliths) within Phanerozoic basins in NE Brazil (Souza et al., 2013; Damaceno et al., 2017). The basaltic intrusions indicate relative weakness along the Afonso Bezerra fault system because failure is necessary to open faults and channel mantle-derived melts to reach the upper crust (Lowrie et al., 1986; Mladenović et al., 2015).

The seismic line and wells indicate that pulses of inversion younger than Neogene-Quaternary occurred in the basin during SF2, and that the rift faults propagated into the postrift units and folded the Miocene and Quaternary strata (Figs. 9, 10). The coastal marine Barreiras Formation reaches an elevation of at least 200 m, which is well above its average elevation of nearly 70 m near the Brazilian coast (Rossetti et al., 2013). The presence of these deposits at elevations up to 250 m asl at sites at the Mel Dome and at depths below the modern sea level in offshore areas indicates a significant variation in height that cannot be explained solely by sedimentation. The Quaternary sediments that cap the Barreiras Formation are at elevations as high as 270 m in the Mel Dome (Fig. 8). The resulting interpretation of these upper postrift layers indicates that the Mel Dome is a broad anticline. In addition, fold hinges near and parallel to the rift faults are consistent with our results and have been described in several oil fields along the eastern rift border faults (Souto Filho et al., 2000). The dome and adjacent alluvial valleys indicate that the Potiguar Basin is currently experiencing tectonic inversion and that the postrift units, mainly those in the central part of the basin, are being uplifted and exhumed. We interpret the Mel Dome as the surface expression of the tectonic squeezing of the basin. We propose that the present-day dome relief and the radial drainage pattern are related to positive tectonic inversion since the Neogene that is caused by a horizontal maximum compression oriented orthogonal to the NE-striking rift faults.

Inversion of the normal faulting stress regime during rifting to a strike-slip stress regime in the postrifting phase was previously proposed for the Araripe (Marques et al., 2014) and Rio do Peixe (Nogueira et al., 2015) basins, which are located 350 km and 200 km south of the equatorial margin, respectively (Fig. 1B). In the Araripe Basin, inversion caused uplift of marine deposits to continental conditions and caused basin dissection by alluvial incision (Marques et al., 2014). Although both basins show evidence of E-W- to ENE-WSW-trending subhorizontal compression, they did not record an initial stress field with N-S-trending subhorizontal compression, such as in the Potiguar Basin. In addition, the stress fields in the Araripe Basin (located 200 km SW of the Potiguar Basin; Fig. 1B) and Rio do Peixe Basin (located 120 km south of the Potiguar Basin; Fig. 1B) in northeastern Brazil inverted from normal stress fields during rifting to strike-slip stress fields during the postrifting phase. This shift occurred from the Late Cretaceous to the Miocene, when the NW-SE-extension transitioned to ENE-WNE horizontal compression. The exact timing of this shift could not be determined due to the lack of temporal markers in these basins (Marques et al., 2014; Nogueira et al., 2015), which is a chronological problem that is resolved by our data.

5.2 The influence of the stress fields on the petroleum system of the Potiguar Basin

The petroleum systems of the Potiguar Basin have two main source units. The first is the lacustrine black shales of the Pendência Formation (rift phase), located onshore in the Potiguar grabens. This source had its peak oil generation during the Campanian, which migrated to the same unit (Mello et al., 1988; Bertani et al., 1990). The second oil source is the marine-evaporite and lacustrine black shales and marls of the Alagamar Formation (transition between rift and postrift), which is responsible for more than 70% of the oil that accumulated in the basin. The oil from this second source was generated in the offshore portion of the basin during the Miocene-Holocene (Souto Filho et al., 2000). This oil migrated along the major fault systems (Figs. 2, 8) and filled the postrift reservoirs of the Alagamar and Açu formations (Fig. 8) until it reached the farthest reservoir in the onshore portion of the basin, more than 100 km from the offshore source (e.g., Mello et al., 1988; Bertani et al., 1990; Souto Filho et al., 2000; Penteado et al., 2007). The present study indicates that the reactivated NE-SW-striking rift faults (Areia Branca and Carnaubais systems; Figs. 2 and 8) played a major role in the migration of oil in the postrift period during the SF1 and SF2 stress fields.

The stress data we present in this study area are consistent with previous descriptions of the traps of the Alagamar-Açu petroleum system in the main reservoirs of the postrift units. Two main NE-SW-striking fault systems that cut across the postrift units concentrate the oil fields: the Areia Branca and the Carnaubais (Fig. 8). Both fault systems are postrift reactivations of major rift fault systems (Bertani et al., 1990). The drag of postrift layers along these fault systems in a strike-slip regime folded and formed anticlines. A shale unit with good lateral continuity at the top of the Açu Formation acted as a regional seal that trapped the oil along the NE-oriented hinges of the anticlines (Souto Filho et al., 2000). The stress data presented in this study indicate that the maximum compressions of both SF1 and SF2 were subhorizontal and oblique to the main NE-SW-striking fault systems, which would induce compression and fold dragging, consistent with the creation of anticlines that formed the traps for the Alagamar-Açu petroleum system. In addition, studies in the basin support the hypothesis that most of the oil generated in the Alagamar Formation migrated along these ENE-WSW-striking fractures that formed and have remained open since the Eocene (Souto Filho et al., 2000). These fractures are consistent with mode-I tensional fractures that formed during SF2, mostly after the Miocene.

A pattern of deformation favorable for hydrocarbon accumulation similar to the one presented in this study was identified by Gomes et al. (2014) in the offshore part of the Potiguar Basin. In addition, Cenozoic anticlines related to mass movements were identified, for example, by Kruger et al. (2012) in the Barreirinhas Basin and Pellegrini and Ribeiro (2018) in the Pará Maranhão Basin (Fig. 1A). Despite the difference in the deformation mechanism of these mass movements compared to those described in the present study, these anticlines are the likely sites for hydrocarbon accumulation.

5.3 Origin of the stress fields and implications for reconstructing the postrift history of the equatorial margin of South America

The onset of postrift stress fields in the Potiguar Basin is consistent with major events on the equatorial margin and indicates how knowledge of the former can contribute to an understanding of the latter. The deformation and opening of the equatorial Atlantic were diachronous (Szatmari, 2000). However, the chronology of the most important event is well established (Matos, 2000). The passive margin phase of the equatorial margin (drifting) occurred after the end of the thermal effect of a spreading center, when the tectonic influence of the fracture zones had a minor control on the generation of space for sedimentation (stretching phase) (Matos, 2000). The rifting phase mainly occurred in the Aptian-Albian but lasted until the Cenomanian (Matos, 2000). The passive margin stage started in the Cenomanian-Turonian (100-90 Ma), when an oceanic connection between the waters of the central and south Atlantic was established (Antobreh et al., 2009). This period also coincides with the deposition of the first continental postrift units during the Albian-Turonian in the Potiguar, Ceará, and Barreirinhas basins (Matos, 2000; Pessoa Neto et al., 2007). It also coincides with the onset of the first postrift stress field in the Potiguar Basin active since the Campanian (this study).

The origin of both stress fields is a matter of debate. The wrench tectonics after the Cenomanian was characterized by both transpression and transtension along the newly created transform fault zone (Matos, 2000; Szatmari, 2000). We suggest that pulses of transpression could have induced the N-S-trending compression and E-W-trending extension, which generated SF1 from the Campanian to the Paleogene in the Potiguar Basin. However, this hypothesis does not rule out other mechanisms. In addition, SF1, which was not previously recognized in the Potiguar Basin, ended during the deposition of the Barreiras Formation. This unit resulted from a major marine transgression in the Miocene, which is also recorded in several other coastal areas of South America (Rossetti et al., 2013). The end of this transgression was marked by unconformities in several sedimentary basins along the Brazilian continental margin (e.g., Pessoa Neto et al., 2007) and West Africa (Fairhead et al., 2013). These unconformities are related to major plate shifts, which led to changes in the stress field (Fairhead et al., 2013). Several studies have related variations in the stress field during the postrift stages to the activity of oceanic fracture zones along the equatorial margins of South America and Africa and major shifts in plate direction (e.g., Davidson et al., 2016).

Another explanation for the end of SF1 and the onset of SF2 is a major plate shift coeval with the end of the Incaic period (50-40 Ma) and the onset of the Quechuan period (22-0 Ma), which are two major phases of the Andean uplift (Garzione et al., 2008). During these periods, the topographic gradients of both the Mid-Atlantic ridge (MAR) and the Andes cordillera have induced intraplate stresses necessary for tectonic inversion in the South America plate (e.g., Assumpção, 1992; Cogné et al., 2012). As a detailed discussion presented by Marques et al. (2014) already indicates, the stresses caused by the Andes and MAR have been transmitted into the interior of the South American plate, which behaves as effectively elastic (Marques et al., 2014).

Based on the ages of the fault-controlled basaltic magmas, which were emplaced as shallow basaltic intrusions (dikes, plugs, laccoliths, and lopoliths), a major peak of fault reactivation occurred at 30-10 Ma. However, the recurrence of basaltic magmatism since the breakup of Pangea (e.g., Fodor and McKee, 1986; Mizusaki et al., 2002; Knesel et al., 2011; Souza et al., 2003, 2013) along the onshore equatorial margin of South America, as well as Pliocene to Pleistocene magmatism in the Fernando de Noronha Archipelago (Perlingeiro et al., 2013), suggests recurring reactivation of the fault systems. This recurrent basaltic magmatism and fault reactivation may be ascribed to a combination of factors as follows: (1) probable synchronicity with Paleogene and Neogene tectonic events along the Andean margin; (2) a thermal anomaly in the shallow upper mantle of northeastern Brazil, as deduced from geophysical data (Pinheiro and Julià, 2014); (3) a permanent state of melting and periodic segregation of small volumes of basaltic melts (Knesel et al., 2011); and (4) upwelling magma flows of small-scale plate-driven convection in the upper mantle (Knesel et al., 2011; Perlingeiro et al., 2013) inherited from the St. Helens hot spot. Thermal anomalies appear to have travelled west with the South American Plate when the St. Helens hot spot became active in the Cretaceous (120-100 Ma) (cf. Nurnberg and Muller, 1991; Wilson and Guiraud, 1992). A combination of hypotheses (2), (3) and (4) is the likely explanation for this recurrent magmatism because they form a series of processes by which magma is stored beneath the crust to form a thermal anomaly and ascends to the upper crust during pulses of faulting.

The transition from SF1 to SF2 in the Potiguar Basin coincides with major events offshore along the equatorial margin. For example, this transition coincides with the shift from gravity gliding with normal faulting near the margin and thrusts at the toe of the continental platform in the Paleogene to E-W-oriented compression on the African and South American side (e.g., Trosdtorf et al., 2007; Davison et al., 2016). The maximum horizontal compression roughly parallel to the equatorial margin during SF2 is consistent with the extensional-compressional tectonics system (an extensional fault system near the continent, a distal contractional system away from the continent, and a transitional or translational domain between the two that affected the sedimentary units from the Late Cretaceous to the Neogene (e.g., Oliveira et al., 2012).

The origin of SF2 is better constrained due to its correspondence with the present-day stress field, which indicates that they a common origin. The fault-slip data are also consistent with the present-day strain derived from GPS data in this basin (Marotta et al., 2015) (Fig. 12). However, in contrast to SF2, the normal faults in the current stress field are mainly located in the central part of the basin and extend to a depth of 2 km (Reis et al., 2013). This apparent contradiction is consistent with the doming in the main graben area.

The shift of S_{Hmax} from E-W- to NW-SE in the present-day stress field roughly following the coastline in the central part of the basin was related to the contrast in density between the continental and oceanic crust (Assumpção, 1992; Ferreira et al., 1998). This maximum compressive stress (σ_1) that has been parallel to the continental margin of the Potiguar Basin since the Miocene has also been observed in other passive margins (e.g., Santimano and Rillen, 2011). Away from the continental margin, however, SF2 continues to be a strike-slip regime, but the maximum compression is oriented ENE-WSW (Marques et al., 2014; Nogueira et al., 2015). This change was related to the temporal shift in the stress field due to plate-driving forces in the Andes. This episode coincided with the 22–0 Ma Quechuan period of uplift (Coutand et al., 2001), when the Andean Plateau was exceptionally high (Garzione et al., 2008). A similar stress pattern of σ_1 parallel to the coastline developed with the breakout along the N-S-trending coast of the Sergipe-Alagoas Basin 400 km south of the Potiguar Basin (Lima et al., 1997).

The stress fields recorded in the Potiguar Basin have implications for reconstructing the tectonic history of the continental margin of South America, especially SF2, which matches the present-day stress field. For example, the present-day stress field on the eastern continental margin of South America is characterized by a subhorizontal compressive horizontal stress and a strike-slip to reverse stress regime (Assumpção et al., 2014). This subhorizontal compression on the continental margin of Brazil is comparable to that recorded in the southeastern part of the Australian passive margin and along the West African margin (Hudec and Jackson, 2002), where inversion anticlines indicate major periods of Miocene-Quaternary compression (Schneider et al., 2004; Sharp and Wood, 2004; Hillis et al., 2008).

Repeated fault reactivation and the generation of new faults are manifested in the intraplate seismicity of the area adjacent to the Potiguar Basin (Bezerra and Vita-Finzi, 2000; Bezerra et al., 2011). The orientations of the rift structures in relation to the stress field (Reis et al., 2013), overpressuring of faults (Bezerra et al., 2007), and fault weakening (Bezerra et al., 2007, 2011) in this basin could be evidence of inversion.

Considering the mean elevations of the Barreiras Formation of 67 m asl in the adjacent Paraíba Basin (Rossetti et al., 2013) and more than 250 m asl in the Mel Dome, it is reasonable to infer that more than 180 m of uplift has occurred over the last 23 Ma. This rate is consistent with those found in Miocene-recent anticlines in Australia, where 200 m of uplift has occurred since the early-mid Pliocene (Sandiford et al., 2004). Similar uplift rates are not predicted by the classical postrift evolution model of sedimentary basins (e.g., McKenzie, 1978).

The new data presented in this study help to constrain the changes in stress along the continental margin of Brazil from a vertical to horizontal maximum compressive stress, which is consistent with the stress evolution in intraplate South America. The change in the stress field influenced the present-day landscape and also the Quaternary sedimentary record. The process we describe here might have implications for reconstructing the neotectonic history of the eastern continental margin of South America and other passive margins elsewhere.

6. Conclusion

The stress field evolution of the Potiguar Basin constrains the postrift history of the equatorial margin of Brazil based on the following conclusions:

(a) The well-constrained chronology of sedimentary, volcanic and hypabyssal rocks allowed us to identify two stress fields. After rifting ceased, an intraplate strike-slip stress regime with N-S-trending compression and E-W-trending extension (SF1) occurred from the Late Cretaceous (from at least the Campanian) to the middle Miocene.

(b) Stress field SF1 was replaced by a neotectonic strike-slip stress regime (SF2) with E-W- to NW-SE-trending compression and N-S- to NE-SW-trending extension. Shortening during SF2 has been accommodated by strike-slip and reverse faults and folding of postrift Miocene-Quaternary sedimentary units.

(c) SF2 shaped the topography of the Potiguar Basin and caused doming of the central part of the basin. Basin inversion shaped the drainage basins into a radial pattern at the basin centre.

(d) The onset of the present-day stress field (SF2) occurred at the end of the major peak of volcanism at 30-25 Ma and the beginning of the deposition of the Barreiras Formation at 23-17 Ma.

(e) SF2 continues today and is consistent with stress data from focal mechanisms, borehole breakouts, image logs, and strain data from GPS permanent monitoring.

(f) Both SF1 and SF2 reactivated the major onshore NE-SW-striking rift fault systems and generated anticlines in the postrift units. These anticlines trapped the petroleum of the Alagamar-Açu system that has migrated from offshore marine-evaporitic and lacustrine units in the transitional sequence. The oil migration process mainly occurred during the Campanian and Miocene-Quaternary.

(g) SF1 and SF2 developed in a passive margin stage of the equatorial margin, when the connection between the equatorial Atlantic and South Atlantic was established. This period coincides with the wrenching phase of the equatorial margin.

(h) The multitude of data presented in this study supports post-breakup deformation along the equatorial margin of South America, which is under compression and contains mainly of Neogene- to Quaternary-controlled landforms.

Acknowledgments

We thank Peter Szatmari, Gareth Crutchley, two anonymous reviewers, and Marine and Petroleum Geology editor Tiago Alves for the detailed and positive criticism that greatly improved our study. We also thank the Brazilian Agency of oil and gas (ANP) for the seismic sections and borehole data. This work was funded by the following projects of the Brazilian National Research Council (CNPq): (a) National Institute of Science and Technology on Tectonic Studies (INCT-ET) no. 573713/2008-1, which paid the field costs and VES survey; and (b) Project no. 300371/2014-4, which sponsored a visiting professor grant to Giovanni Bertotti in Brazil. FHRB, DLC, RPM, DFR, and ZSS thank CNPq for their productivity grants.

References

Almeida, F.F.M., Carneiro, C.D.R., Machado Jr., D.L., Dehira, L.K., 1988. Magmatismo pós-Paleozóico no nordeste oriental do Brasil. Revista Brasileira de Geociências. 18, 451–462.

Alves, T.M., Fetter, M., Lima, C., Cartwright, J.A., Cosgrove, J., Gangá, A., Queiroz, C.L., Strugale, M., 2017. An incomplete correlation between pre-salt topography, top reservoir erosion, and salt deformation in deep-water Santos Basin (SE Brazil). Marine and Petroleum Geology 79, 300-320. 10.1016/j.marpetgeo.2016.10.015

Angelier, J., 1979. Determination of the Mean Principal Directions of Stresses for a Given Fault Population. Tectonophysics 56, 17–26.

Angelier, J., 1990. Inversion of field data in fault tectonics to obtain the regional stress—III. A new rapid direct inversion method by analytical means. Geophysical Journal International 103, 363–376.

Angelier J., 1994. Fault slip analysis and paleostress reconstruction. In: Hancock, PL, 1994. Continental Deformation, 1st ed. Pergamon, Oxford.

Antobreh, A.A., Faleide, J.I., Tsikalas, F., Planke, S., 2009. Rift-shear architecture and tectonic development of the Ghana margin deduced from multichannel seismic reflection and potential field data: Marine and Petroleum Geology, v. 26, p. 345–368, doi:10.1016/j.marpetgeo.2008.04.005.

Antunes, A.F., 2004. Evolução Tectono-Estrutural do Campo de Xaréu (Sub-bacia de Mundaú, Bacia do Ceará – NE do Brasil): abordagem multiescala e pluriferramental. Ph.D. Thesis, Programa de Pós-Graduação em Geodinâmica e Geofísica. Universidade Federal do Rio Grande do Norte, Natal, 384 pp.

Arai, M., 1997. Dinoflagelados (Dynophiceae) miocênicos do Grupo Barreiras do nordeste do estado do Pará (Brasil). Revista Universidade de Guarulhos 2, 98–106.

Arai, M., Uesugui, N., Rossetti, D.F., Góes, A.M., 1988. Considerações sobre a idade do Grupo Barreiras no nordeste do Estado do Pará. Proceedings of the Brazilian Geological Congress 35, 738–752.

Araújo, M.G.S., Brito Neves, B.B., Archanjo, C.J., 2001. Idades $^{40}Ar/^{39}Ar$ do magmatismo básico Meso-Cenozóico da Província Borborema Oriental, nordeste do Brasil. Proceedings of the XIX Symposium of Geology of Northeastern Brazil 11, 260–261.

Asmus, H.E., Guazelli, W., 1981. Descrição sumária das estruturas da margem continental brasileira e das áreas oceânicas e continentais, adjacentes - hipóteses sobre o tectonismo causador e implicações para os prognósticos do potencial recursos minerais. Remac Project. Rio de Janeiro: Petrobrás, Centro de Pesquisas e Desenvolvimento, Divisão de Informação Técnica e Propriedade Industrial 9, 187–269.

Assumpção, M., 1992. The Regional Intraplate Stress Field in South America. Journal of Geophysical Research. 97, 11889–11903.

Assumpção, M., Ferrreira, J.M., Barros, L., Bezerra, F.H.R., França, G.S., Barbosa, J.R., Menezes, E., Ribotta, L.C., Pirchiner, M., do Nascimento, A.F., Dourado, J.C., 2014. Intraplate Seismicity in Brazil, in: Ralwani, P. (ed.) Intraplate Earthquakes. Cambridge Univeristy Press, Cambridge, pp. 50–71.

Assumpção, M., Dias F.L., Zevallos, I., Naliboff, J., 2016. Intraplate stress field in South America from earthquake focal mechanisms. Journal of South American Earth Sciences. 71, 278–295.

Azevedo, R.P., 1991. Tectonic evolution of the Brazilian equatorial continental margin basins. PhD Thesis, Imperial College, London, 455 p.

Bertani, R.T., Costa, I.G., Matos, R.M.D., 1990. Evolução tectono-sedimentar, estilo estrutural e habitat do petróleo na Bacia Potiguar, in: Gabaglia, G.P.R., Milani, E.J., (eds.), Origem e Evolução das Bacias Sedimentares. Petrobras, Rio de Janeiro, pp. 291–310.

Bezerra, F.H.R., Vita-Finzi, C., 2000. How active is a passive margin? Paleoseismicity in northeastern Brazil. Geology, 28, 591–594.

Bezerra, F.H.R., Amaral, R.F., Silva, F.O., Sousa, M.O.L., Fonseca, V.P., Vieira, M.M., Moura-Lima, E.N., Aquino, M.R., 2009. Geological Map of the Macau Sheet. Brazilian Geological Survey, 2 maps, 63pp. Brasília, Brazil.

Bezerra, F.H.R., Srivastava, N.K., Sousa, M.O.L., 2014. Geological Map of the Mossoró Sheet. Brazilian Geological Survey, 2 maps, 72pp. Brasília, Brazil.

Bezerra, F.H.R.; do Nascimento, A.F., Ferreira, J.M., Nogueira, F.C., Fuck, R.A., Neves, B.B.B. Sousa, M.O.L., 2011. Review of active faults in the Borborema Province, Intraplate South America Integration of seismological and paleoseismological data. Tectonophysics 510, 269–290.

Bobachev, A.A., 2003. IPI2Win software: http//geophysics.geol.msu.ru/res_labe.htm.

Braun, J., Deschamps, F., Rouby, D., Dauteuil, O., 2013. Flexure of the lithosphere and the geodynamical evolution of non-cylindrical rifted passive margins: Results from a numerical model incorporating variable elastic thickness, surface processes and 3D thermal subsidence. Tectonophysics 604, 72-82.

Boldreel, L.O., Andersen, M.S., 1993. Late Paleocene to Miocene compression in the Faero-Rockall area, in J.R. Parker (ed.), Petroleum Geology of Northwest Europe. Geological Society of London, Special Publication, pp. 1025–1034.

Bott, M. H. P., 1959. The mechanics of oblique slip faulting Geological Magazine 96, 109–117.

Carneiro, C.D.R., Hamza, V.M., Almeida, F.F.M., 1989. Ativação tectônica, fluxo geotérmico e sismicidade no Nordeste Oriental brasileiro. Revista Brasileira de Geociências 19, 310–322.

Cobbold, P.R., Meisling, K.E., Mount, V.S., 2001. Reactivation of an obliquely rifted margin, Campos and Santos Basins, southeastern Brazil. American Association of Petroleum Geology Bulletin 85, 1925–1944.

Cogné, N., Gallagher, K., Cobbold, P.R., Riccomini, C., Gautheron, C., 2012. Post-breakup tectonics in southeast Brazil from thermochronological data and combined inverse forward thermal history modelling. Journal of Geophysical Research 117, B11413. http://dx.doi.org/10.1029/2012JB009340.

Cordani, U.G., 1970. Idade do vulcanismo do Oceano Atlântico Sul. Boletim IAG/USP 1, 9–75.

Coutand, I., Cobbold, P.R., Urreiztieta, M., Gautier, P., Chauvin, A., Gapais, D., Rossello, E.A., López- Gamundí, O., 2001. Style and history of Andean deformation, Puna plateau, northwestern Argentina. Tectonics, 20, 210–234.

Davison, I., Faull, T., Greenhalgh, J., Beirne, E.O., Steel, I., 2016. Transpressional structures and hydrocarbon potential along the Romanche Fracture Zone: a review. In, Nemčok, M., Rybar, S., Sinha, S. T., Hermeston, S. A., Ledvenyiova, L. (eds) Transform Margins: Development, Controls and Petroleum Systems. Geological Society, London, Special Publications, 431, doi.org/10.1144/SP431.2

Damaceno, J.G., de Castro, D.L., Valcácio, S.N., Souza, Z.S., 2017. Magnetic and gravity modeling of a Paleogene diabase plug in Northeast Brazil. Journal of Applied Geophysics 136, 219–230.

Davison, I., Faull, T., Greenhalgh, J., O Beirne, E., Steel, I., 2015. Transpressional structures and hydrocarbon potential along the Romanche Fracture Zone: a review. Geological Society, London, Special Publications 431, 235–248.

De Castro, D.L., Bezerra, F.H.R., 2015. Fault evolution in the Potiguar rift termination, equatorial margin of Brazil. Solid Earth 6, 185–196.

De Castro, D.L., Bezerra, F.H.R., Sousa, M.O.L., Fuck, R.A., 2012. Influence of Neoproterozoic tectonic fabric on the origin of the Potiguar Basin, Northeastern Brazil and its links with West Africa based on gravity and magnetic data. Journal of Geodynamics 54, 29–42.

Dyksterhuis, S., Müller, R.D., Albert,.R.A., 2005. Paleostress field evolution of the Australian continent since the Eocene. Journal of Geophysical Research.110, B05102. doi:10.1029/2003JB002728.

Do Nascimento, A.F., Cowie, P.A., Lunn, R.J., Pearce, R.G., 2004. Spatio-temporal evolution of induced seismicity at Acu reservoir, NE Brazil. Geophysical Journal International 158, 1041–1052.

Doré, A.G., Lundin, E.R., Kusznir, N.J., Pascal, C., 2008. Potential mechanisms for the genesis of Cenozoic domal structures on the NE Atlantic margin: pros, cons and some new ideas, in: Johnson, H., Doré, A.G., Gatliff, R.W., Holdsworth, R.E, Lundin, R., Ritchie, J.D. (eds.), The Nature and Origin of Compression in Passive Margins. Geological Society Special Publication 306, 1–26.

Dyksterhuis, S., Müller, R. D., Albert1, R.A., 2005. Paleostress field evolution of the Australian continent since the Eocene. Journal of Geophysical Research 110, B05102, doi:10.1029/2003JB002728.

Fairhead, J.D., Binks, R.M., 1991. Differential opening of the Central and South Atlantic Oceans and the opening of the West African rift system. Tectonophysics 187, 191—203.

Fairhead, J.D., Green, C.M., Masterton, S.M., Guiraud, R., 2013. The role that plate tectonics, inferred stress changes and stratigraphic unconformities have on the evolution of the West and Central African Rift System and the Atlantic continental margins. Tectonophysics 594, 118–127.

Ferreira, J.M., Oliveira, R.T., Takeya, M.K., Assumpção, M., 1998. Superposition of local and regional stresses in Northeast Brazil: evidence from focal mechanisms around the Potiguar marginal basin. Geophysical Journal International 134, 341–355.

Ferreira, J.M., Bezerra, F.H.R., Sousa, M.O.L., Do Nascimento, A.F., Sá, J.M., França, G.S., 2008. The role of Precambrian mylonitic belts and present-day stress field in the coseismic reactivation of the Pernambuco lineament, Brazil. Tectonophysics. 456, 111–126.

Fodor, R.V., McKee, E.H., 1986. Tertiary basaltic rocks from offshore Northeastern Brazil: geochemistry and K-Ar ages. Anais da Academia Brasileira de Ciências 58, 233–241.

Fodor, R.V., Mukasa, S.B., Sial, A.N., 1998. Isotopic and trace-element indications of lithospheric and astenospheric components in Tertiary alkalic basalts, northeastern Brazil. Lithos 43, 197–217.

Gandini, R., Rossetti, D.F., Netto, R., Bezerra, F.H.R., Góes, A.M. 2014. Neotectonic evolution of the Brazilian northeastern continental margin based on sedimentary facies and ichnology. Quaternary Research 82, 462–472.

Garcia, S., Angelier, J., Bergerat, F., Homberg, C., 2002. Tectonic analysis of an oceanic transform fault zone based on fault-slip data and earthquake focal mechanisms: The Húsavík-Flatey Fault zone, Iceland. Tectonophysics. 344, 157–174.

Garzione, C.N., Hoke, G.D., Libarkin, J.C., Withers, S., MacFadden, B., Eiler, J., Ghosh, P., Mulch, A., 2008. Rise of the Andes 320, 1304–1307.

Gasperini, L., D. Bernoulli, E. Bonatti, A. M. Borsetti, M. Ligi, A. Negri, R. Sartori, and K. von Salis (2001), Lower Cretaceous to Eocene sedimentary transverse ridge at the Romanche Fracture Zone and the opening of the equatorial Atlantic: Marine Geology 176, 101–119.

Gomes, M.P., Vital, H., Bezerra, F.H.R., de Castro, D.L., Macedo, J.W.P., 2014. The interplay between structural inheritance and morphology in the Equatorial Continental Shelf of Brazil. Marine Geology 355, 150–161.

Gunnell, Y., Fleitout, L., 2000. Shoulder uplift of the Western Ghats passive margin, India: A denudational model. Earth Surface Processes and Landforms 23, 391–404.

Gurgel, S.P.P., Bezerra, F.H.R., Corrêa, A.C.B.,Marques, F.O., Maia, R.P., 2013. Cenozoic uplift and erosion of structural landforms in NE Brazil. Geomorphology 186, 68–84.

Hillis, R.R., Sandiford, M., Reynolds, S.D., Quigley, M.C., 2008. Present- day stress, seismicity and Neogene- to- Recent tectonics of Australia's ‘passive’ margins: intraplate deformation controlled by plate boundary forces, in: Johnson, H., Doré, A.G., Gatliff, R.W., Holdsworth, R.E, Lundin, R., Ritchie, J.D. (eds.), The Nature and Origin of Compression in Passive Margins. Geological Society Special Publication 306, 71–90.

Hudec, M., Jackson, M.P.A., 2002. Structural segmentation, inversion, and salt tectonics on a passive margin: Evolution of the Inner Kwanza Basin, Angola. Geological Society of America Bulletin 115, 639–640.

Knesel, K.M., Souza, Z.S., Vasconcelos, P.M., Cohen, B.E., Silveira, F.V., 2011. Young volcanism in the Borborema Province, NE Brazil, shows no evidence for a trace of the Fernando de Noronha plume on the continent. Earth and Planetary Science Letters 302, 38–50.

Krueger, A., Murphy, M., Gilbert, E., Burke1, K., 2012. Deposition and deformation in the deepwater sediment of the offshore Barreirinhas Basin, Brazil. Geosphere 8, 1606–1631; doi:10.1130/GES00805.1.

Lima, C.C., Nascimento, E., Assumpção, M., 1997. Stress orientations in Brazilian sedimentary basins from breakout analysis: implications for force models in the South American plate. Geophysical Journal International 130, 112–124.

Lima, M.G., 2008. A História do intemperismo na Província Borborema, Nordeste do Brasil: Implicações Paleoclimáticas e Tectônicas. PhD thesis, Federal University of Rio Grande do Norte, Natal.

Lima Neto, H.C., Ferreira, J.M., Bezerra, F.H.R., Assumpção, M., Do Nascimento, A.F., Sousa, M.O.L., Menezes, E.A.S., 2013. Upper crustal earthquake swarms in São Caetano: reactivation of the Pernambuco shear zone and trending branches in intraplate Brazil. Tectonophysics 608, 804–811.

Lima Neto, H.C., Ferreira, J.M., Bezerra, F.H.R., Assumpção, M., do Nascimento, A.F., Sousa, MOL, Menezes, EAS, 2014. Earthquake sequences in the Southern block of the Pernambuco Lineament, NE Brazil: stress field and seismotectonic implications. Tectonophys. 633, 21–220.

Lowrie, A., Smoot, C., Batiza, R., 1986. Are oceanic fracture zones locked and strong or weak?: New evidence for volcanic activity and weakness. Geology 14, 242–245.

Marotta, G.S., França, G.S., Monico, J.F.G., Bezerra, F.H.R., Fuck, R.A., 2015. Strain rates estimated by geodetic observations in the Borborema Province, Brazil. Journal of South American Earth Sciences 58, 1–8.

Marques, F.O., Nogueira, F.C.C., Bezerra, F.H.R., De Castro, D.L., 2014. The Araripe Basin in NE Brazil: An intracontinental graben inverted to a high-standing horst. Tectonophysics 630, 251–264.

Maurin, J.C., Guiraud, R., 1993. Basement control in the development of the early cretaceous West and Central African rift system. Tectonophysics 228, 81—95.

Mascle, J., Blarez, E., Marinho, M., 1988. The shallow structures of the Guinea and Ivory Coast Ghana transform margins - their bearing on the equatorial Atlantic Mesozoic evolution. Tectonophysics 155, 193–209.

Matos, R.M.D., 1992. The northeastern Brazilian Rift System. Tectonics 11, 766–791.

Matos, R.M.D., 2000. Tectonic Evolution of the Equatorial South Atlantic. Geophysical Monograph Series 115, 331-354.

McKenzie, D.P., 1978. Some remarks on the development of sedimentary basins. Earth and Planetary Science Letters 40, 25–32.

Mello, M. R., Gaglianone, P. C., Brassell, S. C., Maxwell, J. R., 1988. Geochemical and biological marker assessment of depositional environments using Brazilian offshore oils. Journal of Marine and Petroleum Geology 5, 205–223.

Menezes, M.R.F., Morais Neto, J.M., Szatmari, P., York, D., 2003. Relações cronológicas entre o vulcanismo Macau e a Formação Serra do Martins com base na datação Ar/Ar do plug basáltico "Serrote Preto" (RN, Nordeste do Brasil). Proceedings of the IX Simpósio Nacional de Estudos Tectônicos - III International Symposium on Tectonics 9, 246–249.

Mizusaki, A.M.P., 1989. A Formação Macau na porção submersa da Bacia Potiguar. Boletim de Geociências da Petrobras 3, 191–200.

Mizusaki, A.M.P., Thomaz-Filho, A., Milani, E.J., Césero, P., 2002. Mesozoic and Cenozoic igneous activity and its tectonic control in northeastern Brazil. Journal of South America Earth Sciences 15, 183–198.

Mladenović, A., Trivić, B., Cvetković, V., 2015. How tectonics controlled post-collisional magmatism within the Dinandes: Inferences based on study of tectono-magmatic events in the Kapaonik Mts. (Southern Serbia). Teconophysics 646, 36–49.

Moulin, M., Aslanian, D., Unternehr, P., 2010. A new starting point for the South and Equatorial Atlantic Ocean. Earth-Science Reviews 98, 1–37.

Moura-Lima, E.M., Bezerra, F.H.R., Lima-Filho, F.P., De Castro, D.L., Sousa, M.O.L., Fonseca, V.P, Aquino, M.R., 2011. 3-D geometry and luminescence chronology of

Quaternary soft-sediment deformation structures in gravels, Northeastern Brazil. Sedimentary Geology 235, 160–171.

Müller, R.D., Yatheesh, V., Shuhail, M., 2014. The tectonic stress field evolution of India since the Oligocene. Gondwana Research 28, 612–624.

Nogueira, F.C., Bezerra, F.H.R., Fuck, R.A., 2010. Quaternary fault kinematics and chronology in intraplate Northeastern Brazil. Journal of Geodynamics 49, 79–91.

Nogueira, F.C.C., Marques, F.O., Bezerra, F.H.R., De Castro, D.L., Fuck, R.A., 2015. Cretaceous intracontinental rifting and post-rift inversion in NE Brazil: Insights from the Rio do Peixe Basin. Tectonophysics 644–645, 92–107.

Nurnberg, D., Muller, D., 1991. The tectonic evolution of the South Atlantic Ocean from Late Jurassic to present. Tectonophysics 191, 27–53.

Oliveira, M.J.R., Zalán, P.V., Caldeira, J.L., Tanaka, A., Santarem, P., Trosdtorf Jr., I, Moraes, A., 2012. Linked extensional-compressional tectonics in gravitational systems in the Equatorial Margin of Brazil, in Gao, G. (Ed.), Tectonics and sedimentation: Implications for petroleum systems: AAPG Memoir 100, 159–178.

Ortner, H., Reiter, F., Acs, P., 2002. Easy handling of tectonic data: the programs TectonicVB for Mac and TectonicsFP for Windows. Computer Geosciences 28, 1193–1200.

Pellegrini, B.S., Ribeiro, H.J.P.S., 2018. Exploratory plays of Pará-Maranhão and Barreirinhas basins in deep and ultra-deep waters, Brazilian Equatorial Margin. Brazilian Journal of Geology, 48, 485-502. DOI: 10.1590/2317-4889201820180146

Penteado, H.L.B., Behar, F., Lorant, F., Oliveira, D.C., 2007. Study of biodegradation processes along the Carnaubais trend, Potiguar basin (Brazil) – Part 2. Journal of Organic Chemistry 38, 1197 – 1211. https://doi.org/10.1016/j.orggeochem.2007.03.007

Perlingeiro, G., Vasconcelos, P.M., Knesel, K.M., Thiede, D.S., Cordani, U.G., 2013. 40Ar/39Ar geochronology of the Fernando de Noronha Archipelago and implications for the origin of alkaline volcanism in the NE Brazil. Journal of Volcanology and Geothermal Research 249, 140–154.

Pessoa Neto, O.C., Soares, U.M., Silva, J.G.F., Roesner, E.H., Florêncio, C.P., Souza, C.A.V., 2007. Bacia Potiguar. Boletim de Geociências da Petrobras 15, 357–369.

Petit, J.P., 1987. Criteria for the sense of movement on fault surfaces in brittle rocks. Journal of Structural Geology 9, 597–608.

Pinheiro, A.G., Julià, J., 2014. Normal thickness of the upper mantle transition zone in NE Brazil does not favor mantle plumes as origin for intraplate Cenozoic volcanism. Geophysical Journal International 199**,** 996–1005.

Reis, A.F.C., Bezerra, F.H.R., Ferreira, J.M., Do Nascimento, A.F., Lima, C.C., 2013. Stress magnitude and orientation in the Potiguar Basin, Brazil: Implications on faulting style and reactivation. Journal of Geophysical Research: Solid Earth 118, doi.org/10.1002/2012JB009953.

Rivalenti, G., Mazzucchelli, M., Girardi, V.A.V., Vannucci, R., Barbieri, M.A., Zanetti, A., Goldstein, S.L., 2000. Composition and processes of the mantle lithosphere in northeastern Brazil and Fernando de Noronha: evidence from mantle xenoliths. Contributions to Mineralogy and Petrology 138, 308–325.

Rossetti, D.F., 2004. Paleosurfaces from northeastern Amazonia as a key for reconstructing paleolandscapes and understanding weathering products. Sedimentary Geology 169, 151–174.

Rossetti, DF, Bezerra, FHR, Dominguez, JML, 2013. Late Oligocene-Miocene transgressions along the equatorial and eastern margins of Brazil. Earth-Science Reviews 123, 87–112.

Sandiford, M., Wallace, M., Coblentz, D., 2004. Origin of the in situ stress field in southeastern Australia. Basin Research 16, 325–338.

Santimano, T, Rillen, V., 2011. Kinematics of Tertiary to Quaternary intracontinental deformation of upper crust in the Eastern Central Andes, NW Argentina. Tectonics, 31, TC4002, doi:10.1029/2011TC003068.

Shedlock, K.M., Tanner, J.G., 1999. Seismic hazard map of the western hemisphere. Annals of Geophysics 42, 1199–1214.

Schneider, K.C., Hill, K.C., Hoffman, N., 2004. Compressional growth of the Minerva anticline, Otway Basin, Southeast Australia – evidence of oblique rifting. Journal of the Australian Petroleum Production & Exploration Association 44, 463–480.

Sharp, N.C., Wood, G.R., 2004. Casino Gas Field, offshore Otway Basin, Victoria-the appraisal story and some stratigraphic enlightenment, in: Boult, P. J., Johns, D.R., Land, S.C. (eds), Eastern Australasian Basins Symposium II, Petroleum Exploration Society of Australia, Special Publication.

Sial, A.N., 1976. The post-Paleozoic volcanism of northeast Brazil and its tectonic significance. Anais da Academia Brasileira de Ciências 48, 299–231.

Sial, A.N., 1977. Petrology and mineral chemistry of peridotite nodules included in Tertiary basaltic rocks of northeast Brazil. Geological Society of American Bulletin 88, 1173–1176.

Sial, A.N., Long, L.E., Pessoa, D.A.R., Kawashita, K., 1981. Potassium-argon ages and strontium isotope geochemistry of Mesozoic and Tertiary basaltic rocks, Northeastern Brazil. Anais da Academia Brasileira de Ciências 53, 115–122.

Sippel, J., Wenderoth, M.S., Reicherter, K.R., Mazur, S., 2009. Paleostress states at the south-western margin of the Central European Basin System — Application of fault-slip analysis to unravel a polyphase deformation pattern. Tectonophysics 470, 129–146.

Soares, D.M., Alves, T.M., Terrinha, P., 2012. The breakup sequence and associated lithospheric breakup surface: their significance in the context of rifted continental margins (West Iberia and Newfoundland margins, North Atlantic). Earth and Planetary Science Letters 355-356, 311-326.

Sousa Filho, J.D., Correa, A.C.F., Santos Neto, E.V., Trindade, L.A.F., 2000. Alagamar-Açu petroleum system, onshore Potiguar Basin, Brazil: A numerical approach for secondary migration. American Association of Petroleum Geology Memoir 73, 151–158.

Souto Filho, J.D., Correa, A.C.F., Santos Neto, E.V., Trindade, L.A.F., 2000. Alagamar-Açu petroleum system, onshore Potiguar Basin, Brazil: A numerical approach for secondary migration, in: Mello, M.R., Katz, B.J. (eds.), Petroleum systems of South Atlantic margins. American Association of Petroleum Geology Memoir 73, 51–158.

Souza, Z.S., Vasconcelos, P.M., Nascimento, M.A.L., Silveira, F.V., Paiva, H.S., Dias, L.G.S., Viegas, M.C., Galindo, A.C., Oliveira, M.J., 2004. Geocronologia e geoquímica do magmatismo cretácico a terciário no NE do Brasil. Proceedings of the Brazilian Geological Congress, 42, Araxá, CD-rom.

Souza, Z.S., Nascimento, M.A.L., Barbosa, R.V., Dias, LG.S., 2005. Geology and tectonics of the Boa Vista Basin (Paraíba, northeastern Brazil) and geochemistry of the associated tholeiitic magmatism. Journal of South America Earth Sciences. 18, 391–405.

Souza, Z.S., Kalsbeek, F., Deng, X.D., Frei, R., Kofelt, T.F., Dantas, E.L., Ki, J.W., Pimentel, M.M., Galindo, A.C., 2016. Generation of continental crust in the northern part of the Borborema Province, northeastern Brazil, from Archaean to Neoproterozoic. Journal of South American Earth Sciences, 68, 68–96.

Souza, Z.S., Vasconcelos, P.M., Knesel, K.M., Dias, L.G.S., Rosener, E.H., Farias, P.R.C., Morais Neto, J.M., 2013. The tectonic evolution of Cenozoic extensional basins, northeast Brazil: Geochronological constraints from continental basalt 40Ar/39Ar ages. Journal of South American Earth Sciences 48, 159–172.

Souza, Z.S., Vasconcelos, P.M.P., Nascimento, M.A.L., Silveira, F.V., Paiva, H.S., Dias, L.G.S., Thiede, D., Carmo, I.O., 2003. $^{40}Ar/^{39}Ar$ geochronology of Mesozoic and Cenozoic magmatism in NE Brazil. Short Papers-IV South Amer. Symposium on Isotope Geol, Proceedings 691–694.

Szatmari, P., 2000. Habitat of Petroleum Along the South Atlantic Margins. In: Mello, M.R., Katz, B.J. (eds.). Petroleum systems of South Atlantic margins: American Association of Petroleum geologists Memoir 73, 69-75.

Takeya, M.K., Ferreira, J.M., Pearce, R.G., Assumpção, M., Costa, J.M., Sophia, C.M., 1989. The 1986-1989 intraplate earthquake sequence near João Câmara, northeastern Brazil - Evolution of seismicity. Tectonophysics 167, 117–131.

Trosdtorf, I., Jr, Zalan, P. V., Figueiredo, J.J.P., Soares, E. F., 2007. Bacia de Barreirinhas. Boletim Geociências Petrobras 15, 331–333.

Van Schmus, W.R., Brito Neves, B.B., Hackspacher, P.C., Babisnski, M., 1995. U/Pb and Sm/Nd studies of eastern Borborema Province, northeastern Brazil: initial conclusions. Journal of South American Earth Sciences 8, 267–288.

Wilson, M., Guiraud, R., 1992. Magmatism and rifting in Western and Central Africa from Late Jurassic to Recent times. Tectonophysics 213, 1–23.

Withjack, M.O., Olsen, P.E., Schlisch, , .W., 1995. Tectonic evolution of the Fundy rift basin, Canada: Evidence of extension and shortening during passive margin development. Tectonics 14, 390–405.

Figure Captions

Figure 1 – (A) Topographic map of the Brazilian Equatorial Margin, showing the main marginal basins (topography from the Global Relief Model from ETOPO1 – NOAA, www.ngdc.noaa.gov/mgg/global/). The black line marks the coastline. (B) Map of the present-day stress data of the eastern part of the Brazilian Equatorial margin superposed on a shaded image derived from the digital elevation model of the shuttle radar topography mission. Stress indicators are focal mechanisms (Assumpção, 1992; Ferreira et al., 1998, 2008; Bezerra et al., 2011; Lima Neto et al., 2014; Oliveira et al., 2015), borehole breakouts (Lima et al., 1997), and image logs (Reis et al., 2013). Sedimentary basins quoted in the text: Potiguar (Pb), Ceará (Ceb), Araripe (Ab), Rio do Peixe (RPb), Parnaíba (Pnb), Iguatu (Igb), Paraíba (Pab), Pernambuco (Peb), Barreirinhas (Bab). Inset: South American continent with location of the study area.

Figure 2 – Simplified tectonic structures and stratigraphy of the Potiguar Basin. A) Simplified geological map with main structures of the rift phase. These structures mostly occur below the post-rift units but are marked on the map for the sake of clarity. B) Cross-section of the central part of the basin (modified from Bertani et al., 1990; Bezerra et al., 2000, 2011).

Figure 3 – Histogram of ages of the Macau volcanism in the Potiguar Basin and adjacent Precambrian basement. Ages sources listed in Table 1.

Figure 4 – Observed and calculated resistivity curves and geoelectrical models obtained from 1D inversion of VES 1, 12, 21, and 30, respectively.

Figure 5 – Paleostress tensors of the stress field 1 (SF1) in the Potiguar Basin. Fault-slip data are shown in equal-area lower hemisphere stereonets. Fault planes = continuous lines and striaes; arrows on the circles = sense of movements of hanging walls (double arrows for strike-slip; inward directed arrows for reverse slip; outward directed arrows for normal slip). Stress tensors of maximum compressive (S1), intermediate (S2), and minimum stresses (S3) as five-red, four-green, and three-blue stars, respectively. Black arrows outside stereonets = directions of compression and extension. Summary of paleostress tensors of SF1 at the upper right-hand corner.

Figure 6 - Paleostress tensors of the stress field 2 (SF2) in the Potiguar Basin. Fault-slip data are shown in equal-area lower hemisphere stereonets. Fault planes = continuous lines and striaes; arrows on the circles = sense of movements of hanging walls (double arrows for strike-slip; inward directed arrows for reverse slip; outward directed arrows for normal slip). Stress tensors of maximum compressive (S1), intermediate (S2), and minimum stresses (S3) as five-red, four-green, and three-blue stars, respectively. Black arrows outside stereonets = directions of compression and extension. Summary of SF2 stress tensors at the right-hand corner.

Figure 7 – Fault pattern and Cenozoic volcanic intrusions in the eastern and central area of the Potiguar Basin on a background of a digital elevation model from the Shuttle Radar Topographic Mission (SRTM). A) Volcanic bodies aligned along the NW-SE-striking Afonso Bezerra fault system. B) Details of a volcanic body along which a right-lateral displacement of the boundary between the Açu and Jandaíra formations occurs. Number of volcanic bodies on the map corresponds to site numbers presented on Table 1. The solid black lines mark the boundaries between units in the Potiguar Basin. See Figure 2 for location. Fault traces and location of volcanic bodies from Bezerra et al. (2009). The bracket black lines on both maps indicate the segments of the Afonso Bezerra fault system. Key: 1, Serra Preta basaltic body; 2, Serra Aguda plug.

Figure 8 – Major faults generated during the Potiguar Basin rifting (white lines), and location of seismic sections, wells and geoelectric survey superposed on a digital elevation model (DEM) from the Shuttle Radar Topography Mission (SRTM). Blue lines = seismic lines (L); yellow triangles = vertical geoelectric soundings (W). Volcanic dome, VD; Mel dome, MD; Assu valley, AV; Mossoró valley, MV. Rift faults after Bertani et al. (1990), Matos (1992), and Souto Filho (2000). The yellow areas indicate the location of the main oil fields in the postrift unit, the Açu Formation (Bertani et al., 1990). Location of area in Fig. 2.

Figure 9 – Seismic sections orthogonal to faults generated during the rifting and reactivated in the postrift phase of the Potiguar Basin. A) Seismic section L 039. B)

Seismic section L 217. C) Seismic section L 194. In each section, a detail of the seismic pattern and the corresponding interpretation are presented on the lower part of each seismic line. (U) mark the unconformity between the rift and postrift sequences. (a’), (b’), (c’) are uninterpreted and (a’’), (b’’), (c’’) are interpreted details of the sections (A), (B), (C), respectively. Location of sections in Figure 8.

Figure 10 – Geoelectric pseudo-section along the Mel dome based on 30 vertical electric soundings (VES) down to a 250-300 m depth (EDI: Estimated Depth of Investigation) that were combined with well data to allow inferences down to a 600 m depth. The topography of the dome was derived from a digital elevation model of the shuttle radar topographic mission data (DEM-SRTM). Location of VESs in Figure 8.

Figure 11 - Topography of the Mel dome and adjacent Quaternary alluvial valleys. A) View from the north. B) View from the north, including radial drainage system. Key: Assu valley, AV; Mel dome, MD; Mossoró valley, MV.

Figure 12 – Maps with the summary of the three stress fields, highlighting the maximum horizontal directions of compression and extension and fault kinematics. A) Stress field 1. B) Stress field 2. C) Present-day stress field.

Figure 12 – Maps with the summary of the three stress fields, highlighting the maximum horizontal directions of compression and extension and fault kinematics. A) Stress field 1. B) Stress field 2. C) Present-day stress field.

Figure 1
Click here to download high resolution image

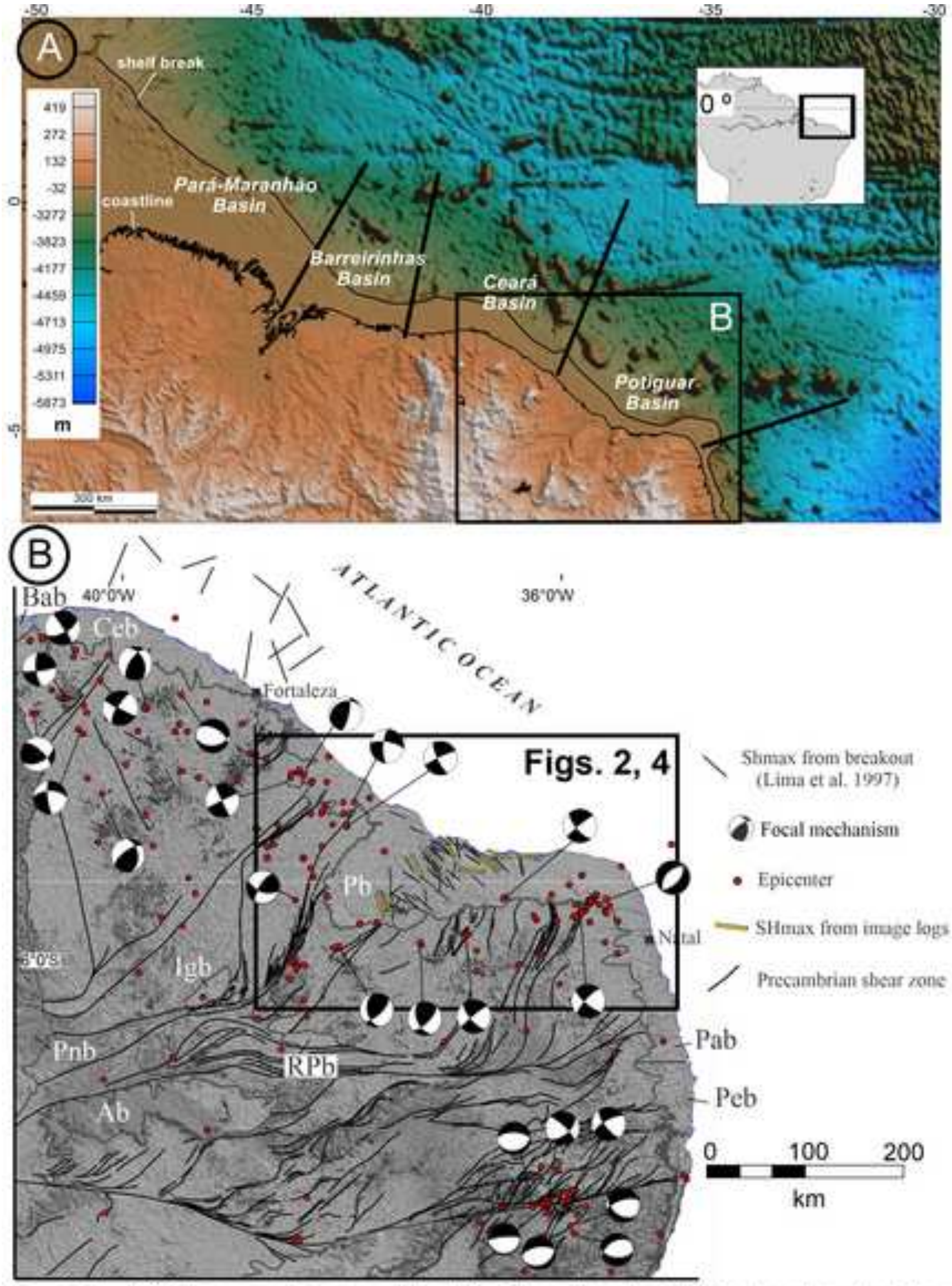

Figure 1 – (A) Topographic map of the Brazilian Equatorial Margin, showing the main marginal basins. (topography from the Global Relief Model from ETOPO1 – NOAA, www.ngdc.noaa.gov/mgg/global/). (B) Map of the present-day stress data of the eastern part of the Brazilian Equatorial margin superposed on a shaded image derived from the digital elevation model of the shuttle radar topography mission. Stress indicators are focal mechanisms (Assumpção, 1992; Ferreira et al., 1998, 2008; Bezerra et al., 2011; Lima Neto et al., 2014; Oliveira et al., 2015), borehole breakouts (Lima et al., 1997), and image logs (Reis et al., 2013). Sedimentary basins quoted in the text: Potiguar (Pb), Ceará (Ceb), Araripe (Ab), Rio do Peixe (RPb), Parnaíba (Pnb), Iguatu (Igb), Paraíba (Pab), Pernambuco (Peb), Barreirinhas (Bab). Inset: South American continent with location of the study area.

Figure 2
Click here to download high resolution image

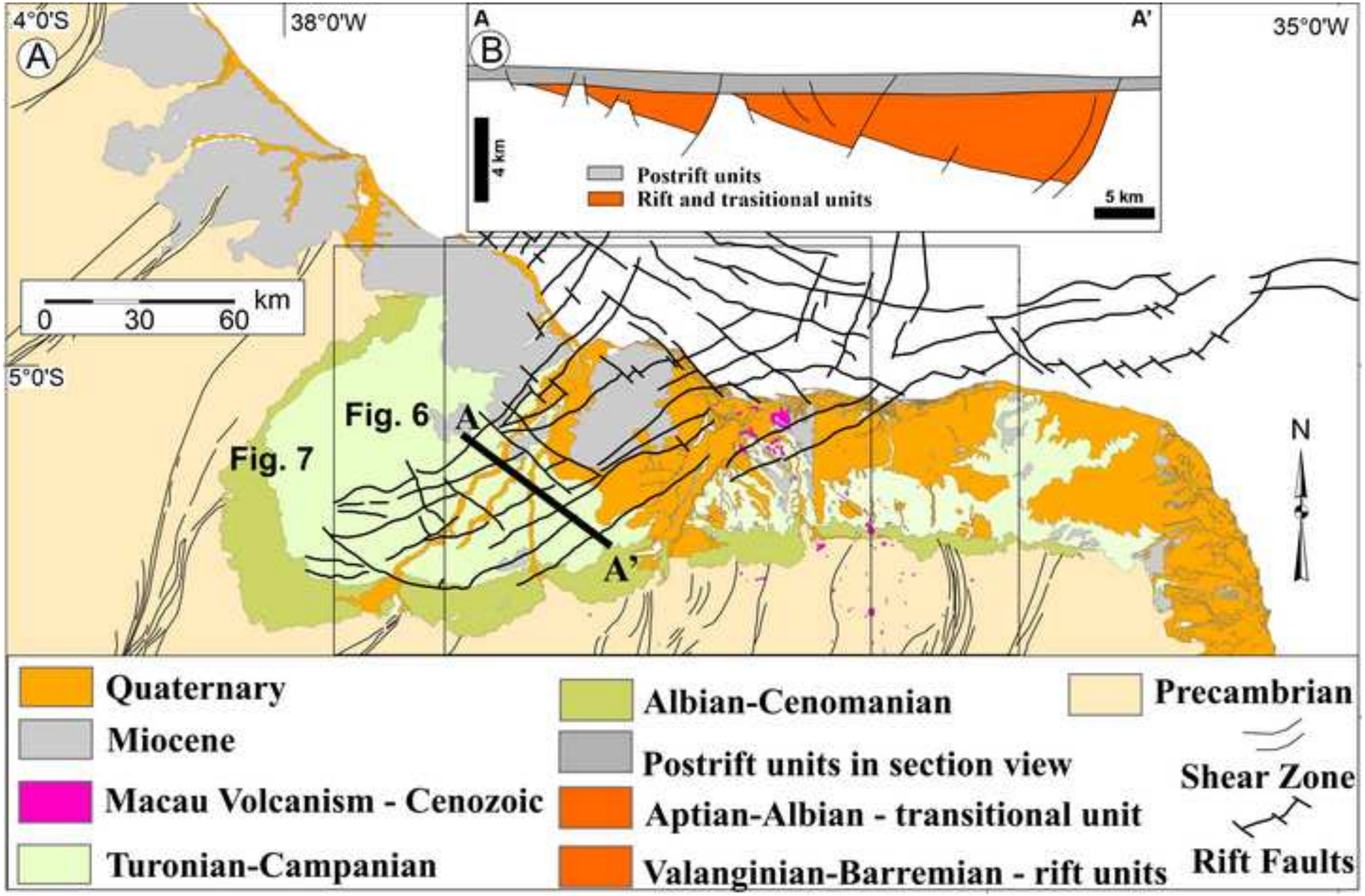

Figure 2 – Simplified tectonic structures and stratigraphy of the Potiguar Basin. A) Simplified geological map with main structures of the rift phase. These structures mostly occur below the post-rift units but are marked on the map for the sake of clarity. B) Cross-section of the central part of the basin (modified from Bertani et al., 1990; Bezerra et al., 2000, 2011).

Figure 3
Click here to download high resolution image

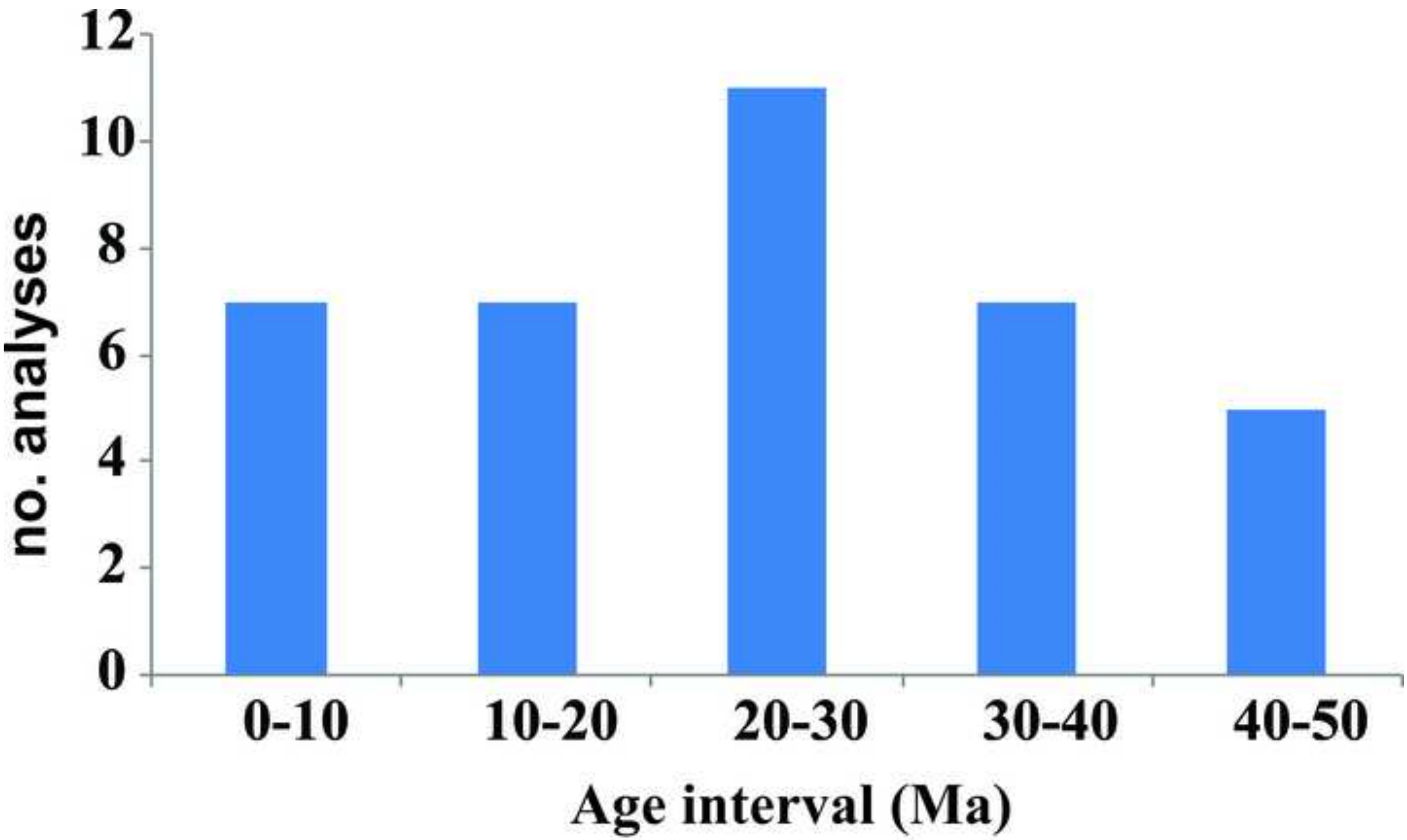

Figure 3 – Histogram of ages of the Macau volcanism in the Potiguar Basin and adjacent Precambrian basement. Ages sources listed in Table 1.

Figure 4

Click here to download high resolution image

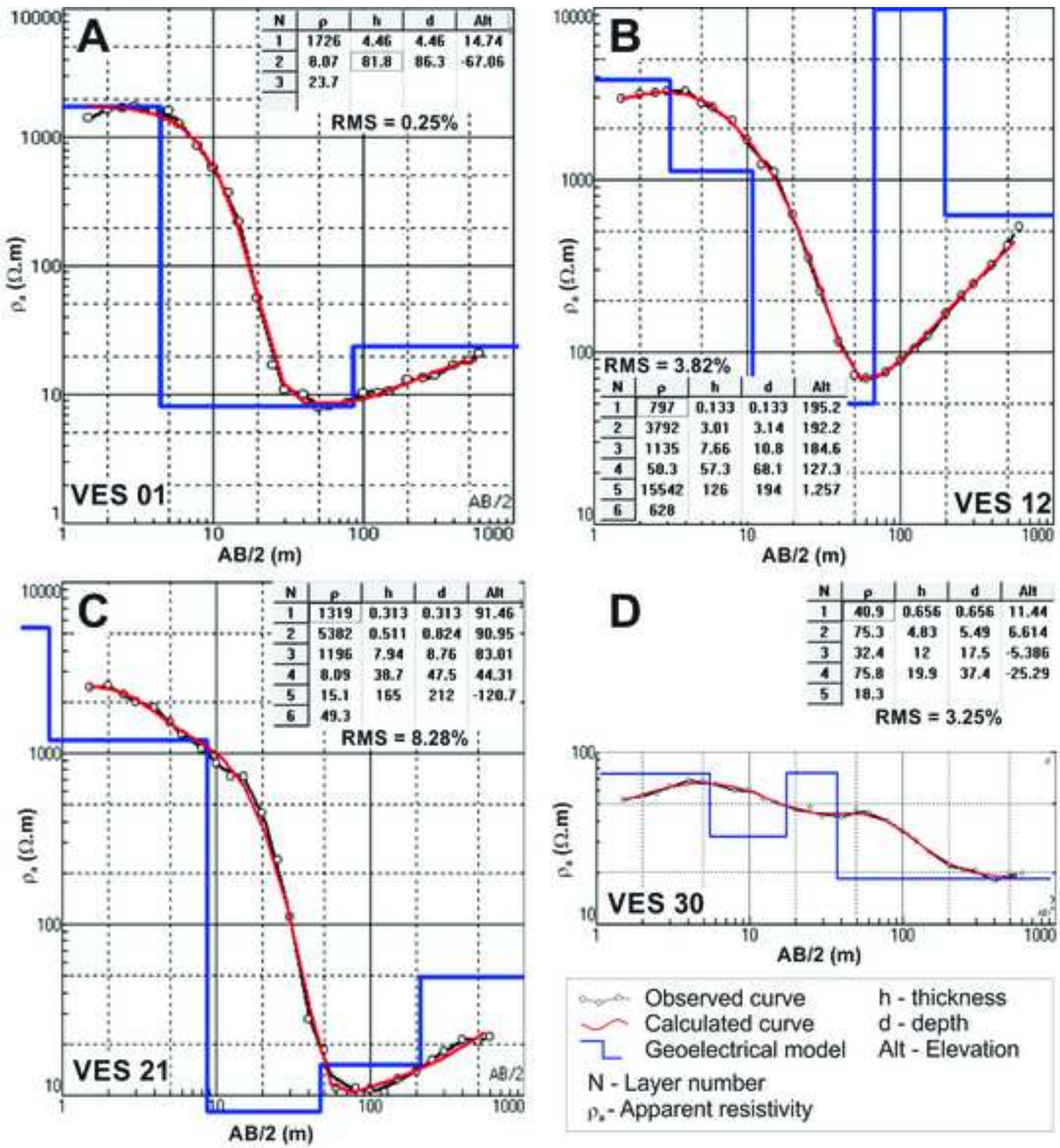

Figure 4 – Observed and calculated resistivity curves and geoelectrical models obtained from 1D inversion of VES 1, 12, 21, and 30, respectively.

Figure 5
Click here to download high resolution image

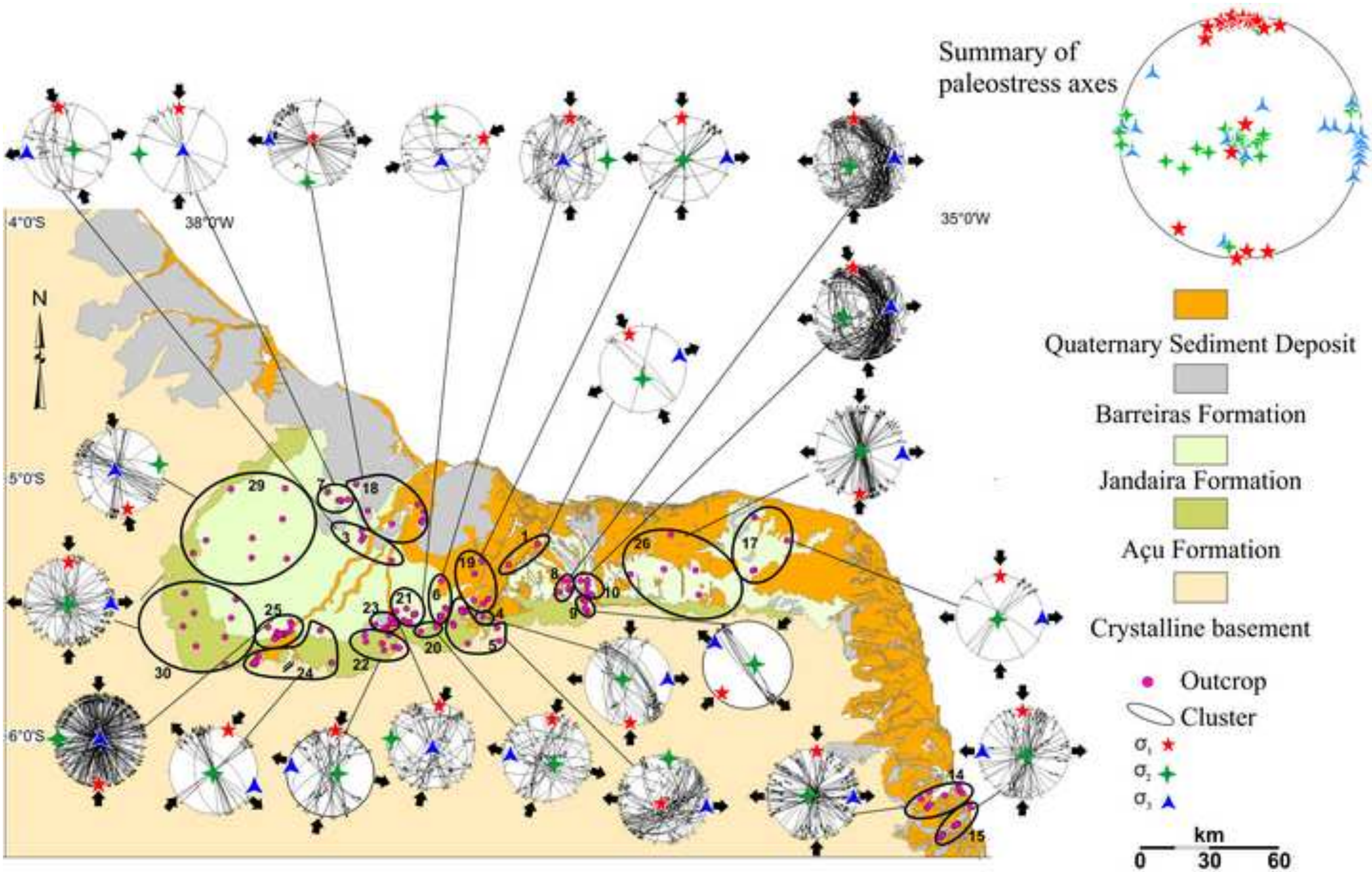

Figure 5 – Paleostress tensors of the stress field 1 (SF1) in the Potiguar Basin. Fault-slip data are shown in equal-area lower hemisphere stereonets. Fault planes = continuous lines and striaes; arrows on the circles = sense of movements of hanging walls (double arrows for strike-slip; inward directed arrows for reverse slip; outward directed arrows for normal slip). Stress tensors of maximum compressive (S1), intermediate (S2), and minimum stresses (S3) as five-red, four-green, and three-blue stars, respectively. Black arrows outside stereonets = directions of compression and extension. Summary of paleostress tensors of SF1 at the upper right-hand corner.

Figure 6

Click here to download high resolution image

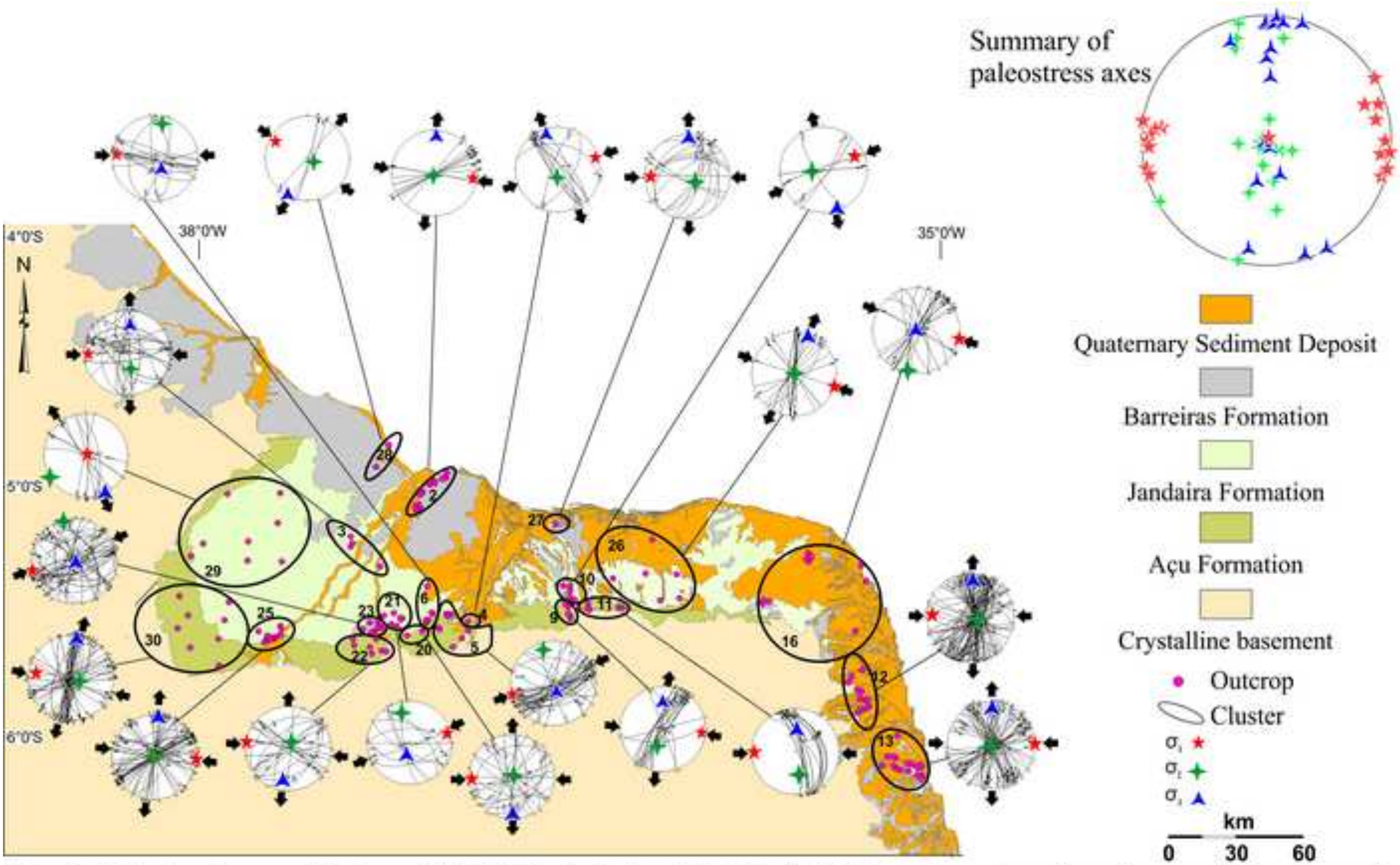

Figure 6 - Paleostress tensors of the stress field 2 (SF2) in the Potiguar Basin. Fault-slip data are shown in equal-area lower hemisphere stereonets. Fault planes = continuous lines and striaes; arrows on the circles = sense of movements of hanging walls (double arrows for strike-slip; inward directed arrows for reverse slip; outward directed arrows for normal slip). Stress tensors of maximum compressive (S1), intermediate (S2), and minimum stresses (S3) as five-red, four-green, and three-blue stars, respectively. Black arrows outside stereonets = directions of compression and extension. Summary of SF2 stress tensors at the right-hand corner.

Figure 7
Click here to download high resolution image

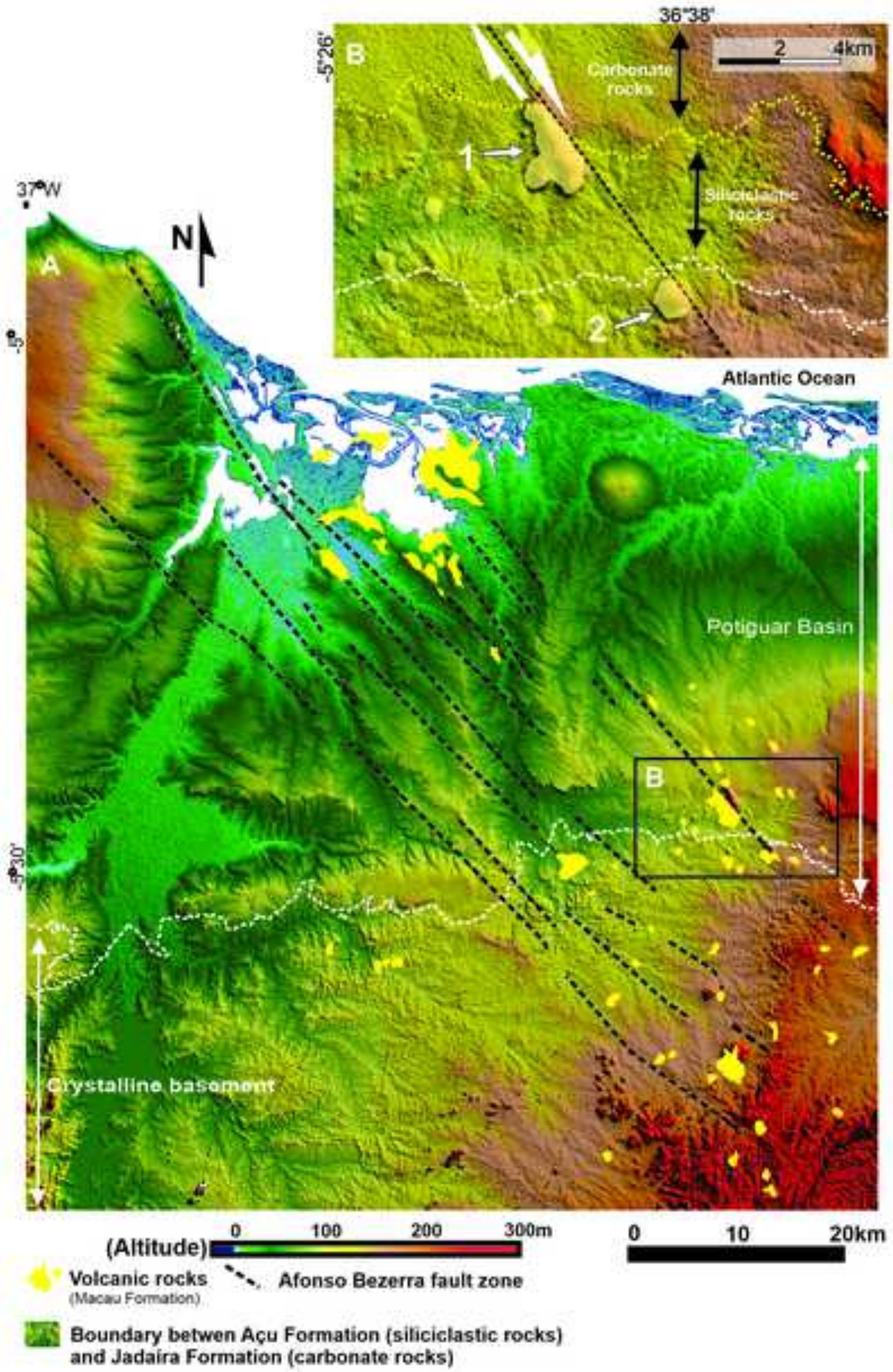

Figure 7 – Fault pattern and Cenozoic volcanic intrusions in the eastern and central area of the Potiguar Basin on a background of a digital elevation model from the Shuttle Radar Topographic Mission (SRTM). A) Volcanic bodies aligned along the NW-SE-striking Afonso Bezerra fault system. B) Details of a volcanic body along which a right-lateral displacement of the boundary between the Açu and Jandaíra formations occurs. Number of volcanic bodies on the map corresponds to site numbers presented on Table 1. See Figure 2 for location. Fault traces and location of volcanic bodies from Bezerra et al. (2009). Key: 1, Serra Preta basaltic body; 2, Serra Aguda plug.

Figure 8
Click here to download high resolution image

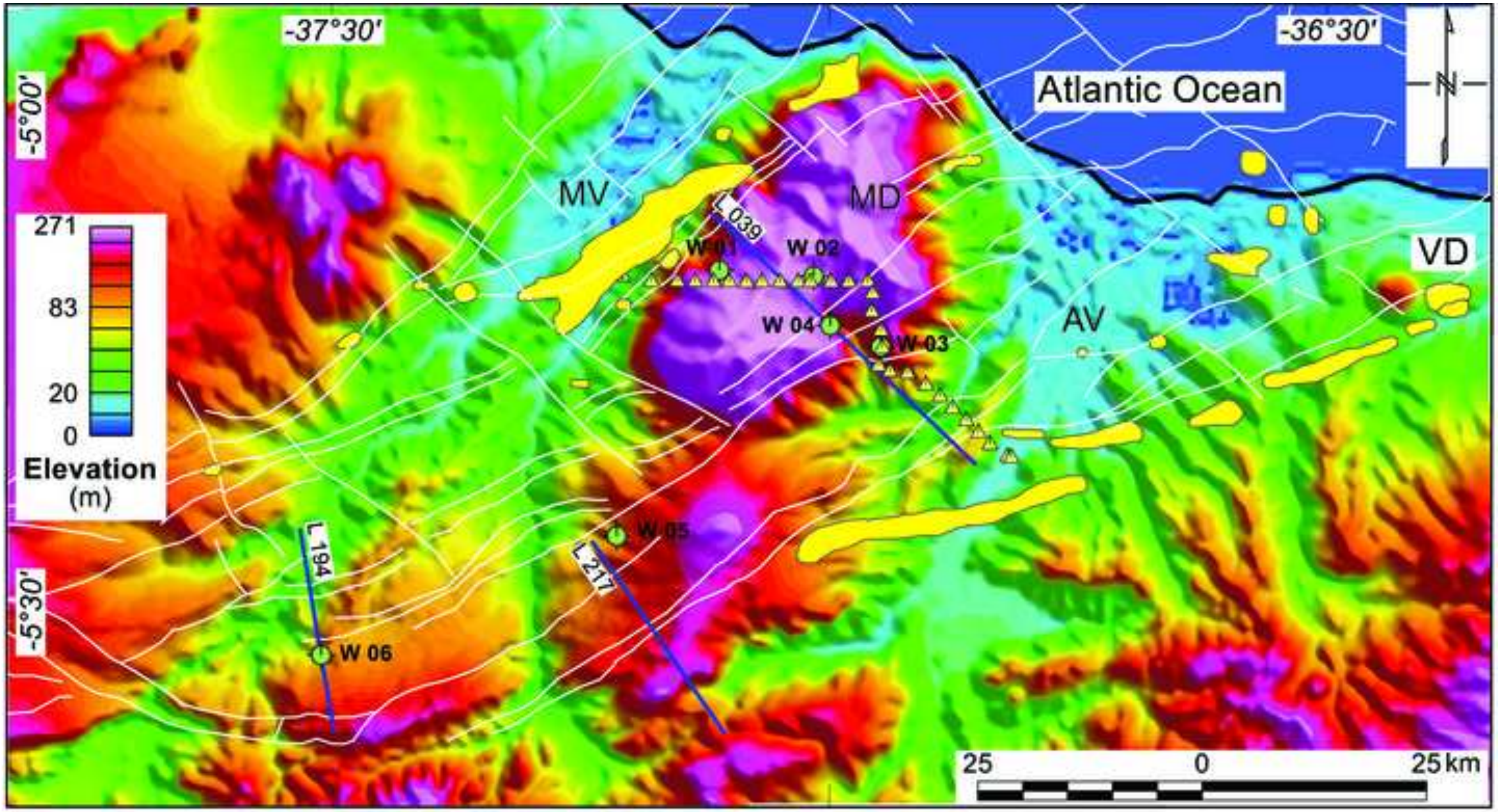

Figure 8 – Major faults generated during the Potiguar Basin rifting (white lines), and location of seismic sections, wells and geoelectric survey superposed on a digital elevation model (DEM) from the Shuttle Radar Topography Mission (SRTM). Blue lines = seismic lines (L); yellow triangles = vertical geoelectric soundings (W). Volcanic dome, VD; Mel dome, MD; Assu valley, AV; Mossoró valley, MV. Rift faults after Bertani et al. (1990), Matos (1992), and Souto Filho (2000). The yellow areas indicate the location of the main oil fields in the postrift unit, the Açu Formation (Bertani et al., 1990). Location of area in Fig. 2.

Figure 9

Click here to download high resolution image

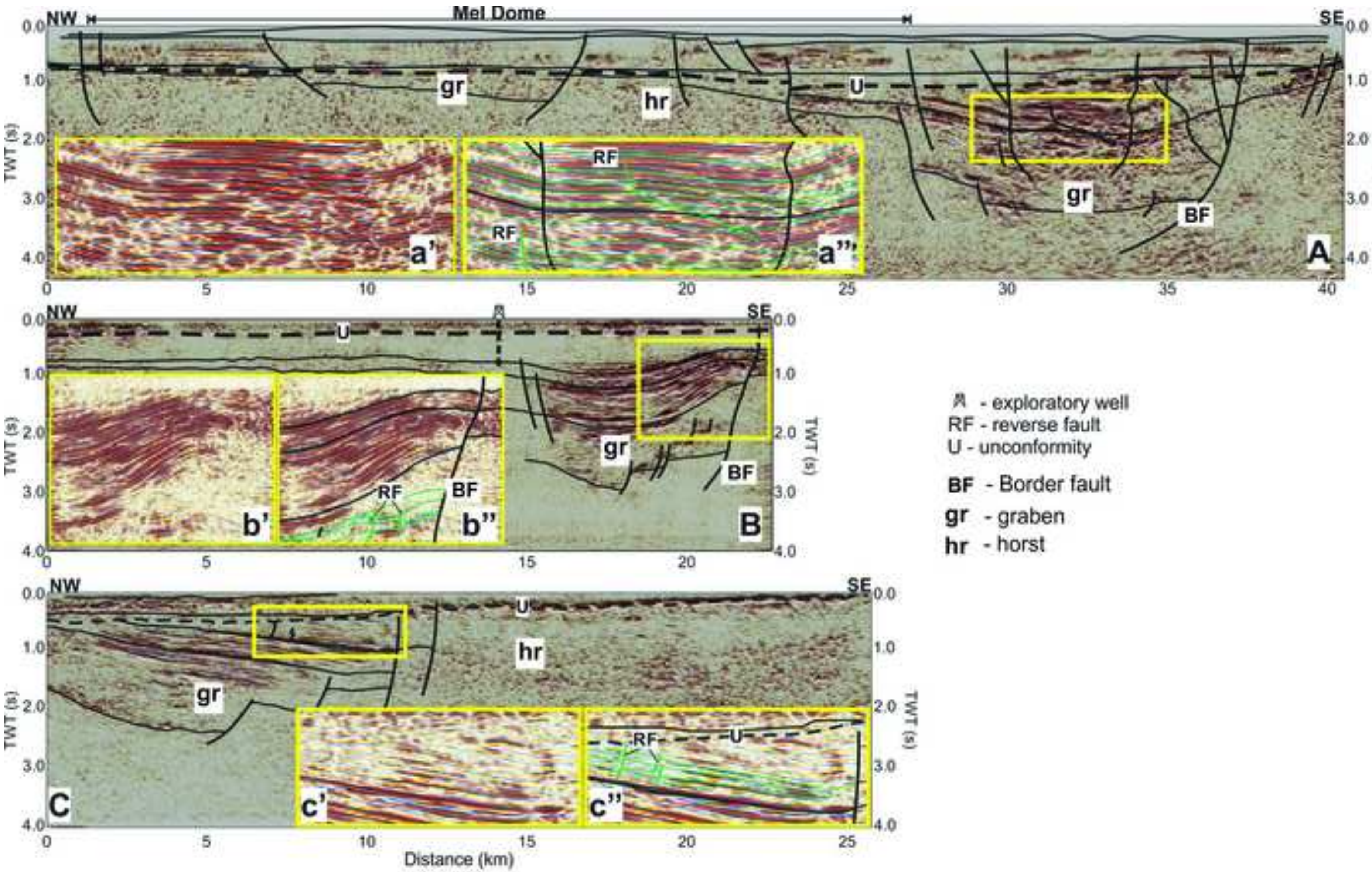

Figure 9 – Seismic sections orthogonal to faults generated during the rifting and reactivated in the postrift phase of the Potiguar Basin. A) Seismic section L 039. B) Seismic section L 217. C) Seismic section L 194. In each section, a detail of the seismic pattern and the corresponding interpretation are presented on the lower part of each seismic line. (U) mark the unconformity between the rift and postrift sequences. (a'), (b'), (c') are uninterpreted and (a''), (b''), (c'') are interpreted details of the sections (A), (B), (C), respectively. Location of sections in Figure 8.

Figure 10
Click here to download high resolution image

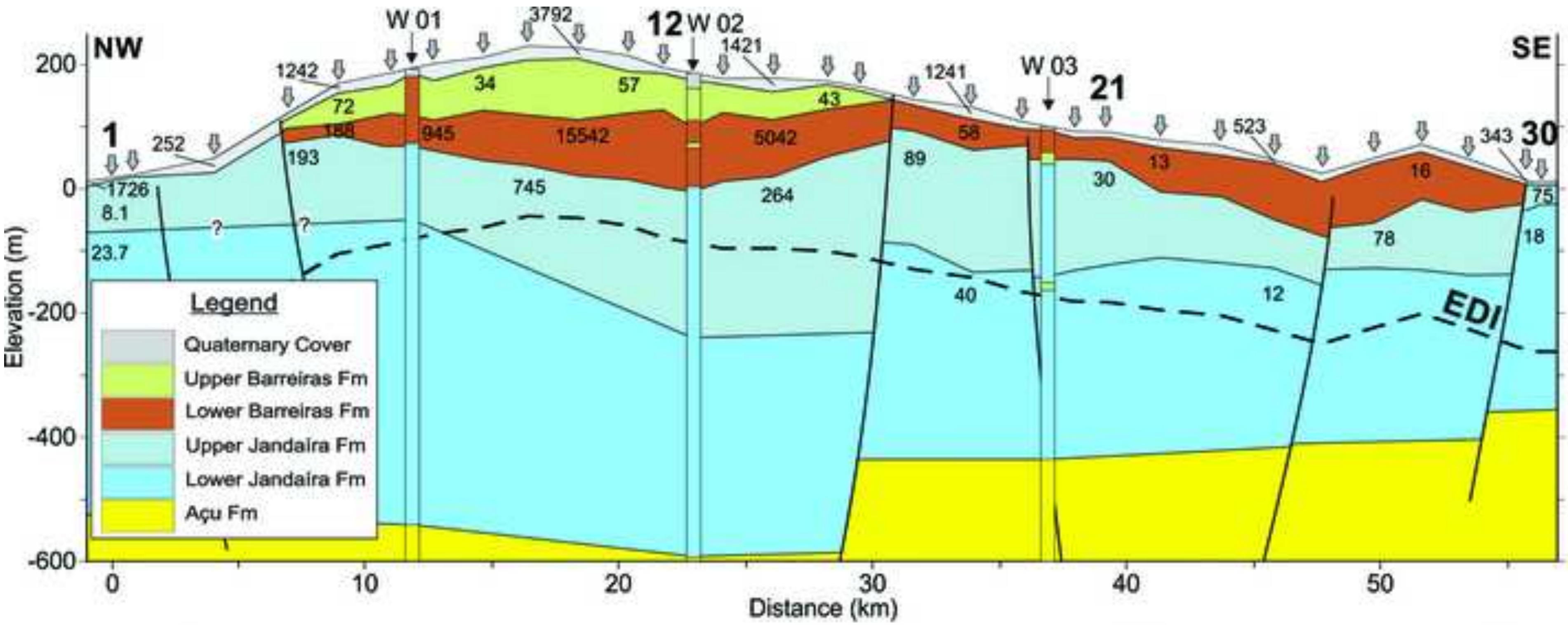

Figure 10 – Geoelectric pseudo-section along the Mel dome based on 30 vertical electric soundings (VES) down to a 250-300 m depth (EDI: Estimated Depth of Investigation) that were combined with well data to allow inferences down to a 600 m depth. The topography of the dome was derived from a digital elevation model of the shuttle radar topographic mission data (DEM-SRTM). Location of VESs in Figure 8.

Figure 11
Click here to download high resolution image

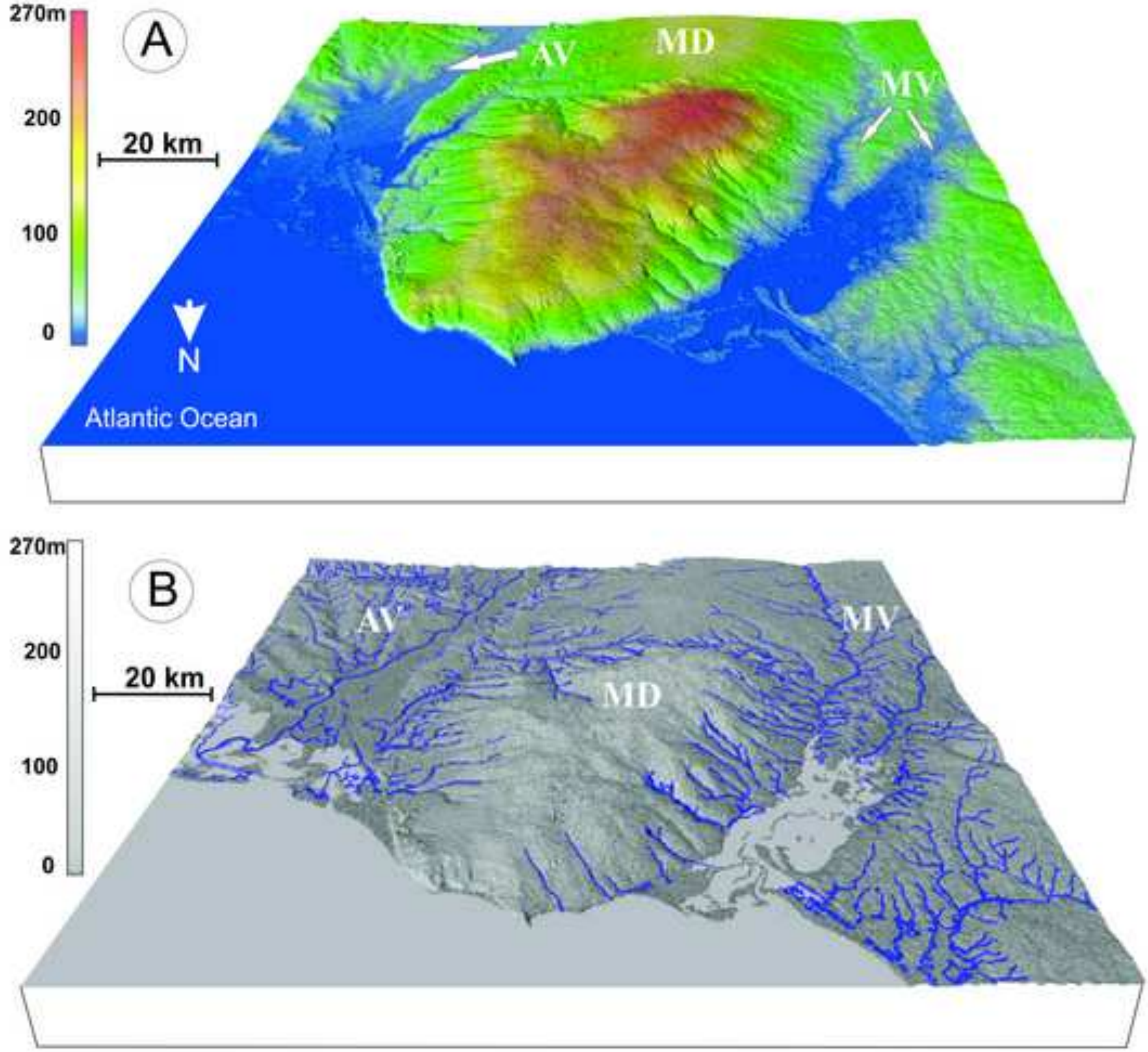

Figure 11 - Topography of the Mel dome and adjacent Quaternary alluvial valleys. A) View from the north. B) View from the north, including radial drainage system. Key: Assu valley, AV; Mel dome, MD; Mossoró valley, MV.

Figure 12

Click here to download high resolution image

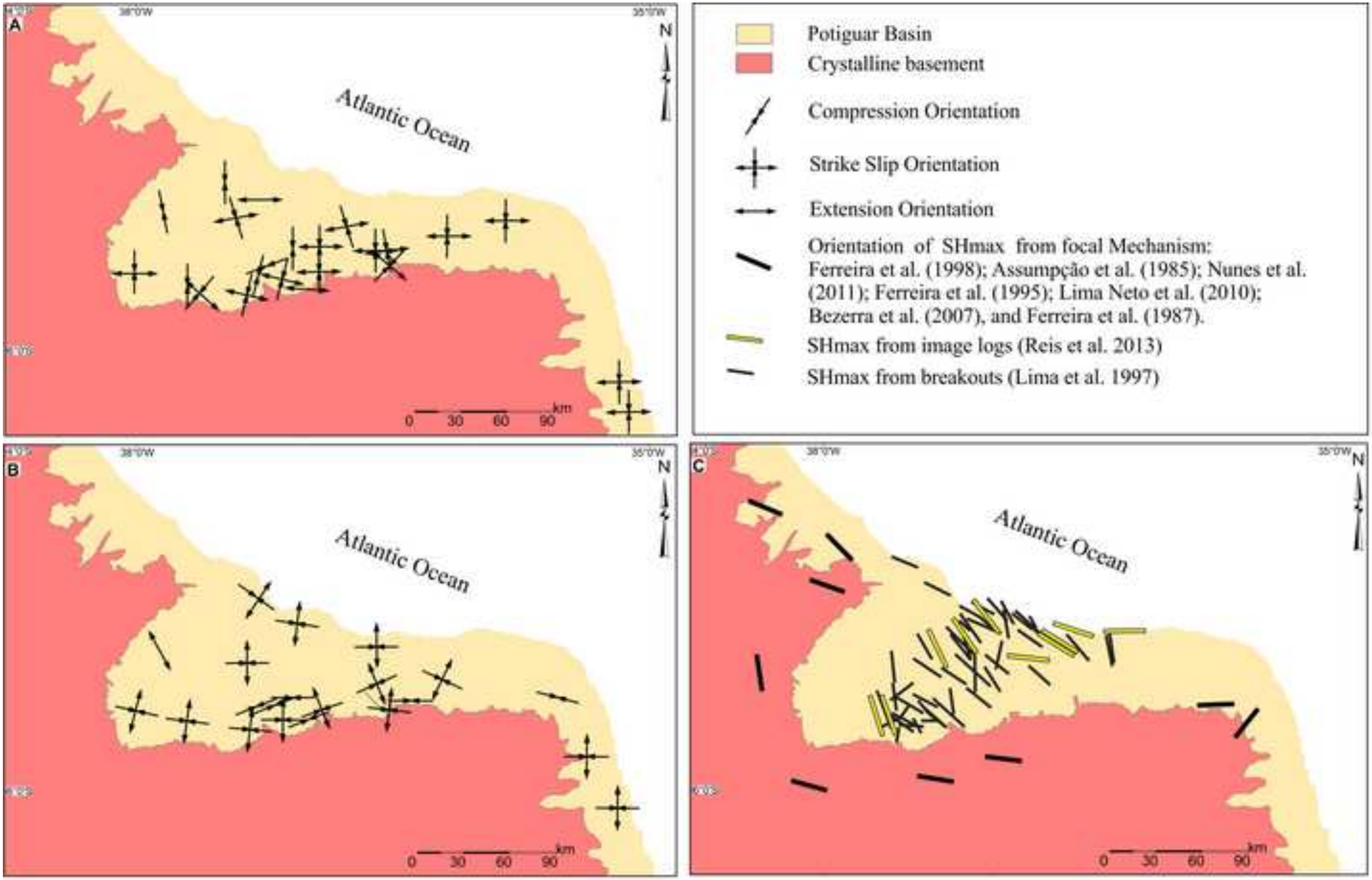

Figure 12 – Maps with the summary of the three stress fields, highlighting the maximum horizontal directions of compression and extension and fault kinematics. A) Stress field 1. B) Stress field 2. C) Present-day stress field.

Table 1

Table 1 – Summary of K/Ar and $^{40}Ar/^{39}Ar$ ages (2-sigma error) of Cenozoic basaltic rocks in the Potiguar Basin and adjacent basement. All ages are from whole rock samples, except for offshore sites, which are feldspar ages.

Site	Lithology	Age	Latitude South	Longitude West	Source
Onshore					
1	Basalt	42.0±3.0[(a)]	05.08.00	36.30.45	Asmus and Guazelli (1981)
2	Basalt	14.2±1[(a)]	05.10.38	36.42.49	Sial et al. (1981)
3	Basalt	18.0±1.0[(a)]	05.20.40	36.20.15	Asmus and Guazelli (1981)
4	Basalt	18.0±0.5[(a)]	05.27.20	36.18.00	Ebert and Brochini (1968) apud Sial (1976)
5	Basalt	12.5±1.0[(a)]	05.28.12	36.19.12	Sial et al. (1981)
5	Basalt	13.0±1.0[(a)]	05.28.12	36.19.12	Sial et al. (1981)
5	Basalt	13.9±2.0[(a)]	05,28,12	36.19.12	Sial et al. (1981)
6	Basalt	24.0±6.0[(a)]	05.30.25	36.20.25	Asmus and Guazelli (1981)
7	Basalt	8.9±0.5[(b)]	05.38.34	36.20.01	Knesel et al. (2011)
8	Basalt	7.5±0.3[(b)]	05.46.06	36.17.49	Knesel et al. (2011)
8	Basalt	7.6±0.4[(b)]	05.46.30	36.17.48	Knesel et al. (2011)
9	Basalt	27.7±0.6[(a)]	05.46.38	36.24.16	Sial et al. (1981)
9	Basalt	7.9±0.3[(b)]	05.47.37	36.26.14	Knesel et al. (2011)
10	Basalt	20.0±1.0[(a)]	05.40.10	36.20.00	Asmus and Guazelli (1981)
11	Basalt	24.6±0.8[(b)]	05.42.05	36.19.15	Souza et al. (2003)
11	Basalt	23.7±1.2[(b)]	05.42.05	36.19.15	Araújo et al. (2001)
11	Basalt	19.7±0.8[(a)]	05.42.05	36.19.15	Cordani (1970)
12	Basalt	24.2±0.3[(b)]	05.58.40	36.13.45	Menezes et al. (2003)
13	Basalt	31.7±1.0[(a)]	05.58.00	36.21.49	Sial et al. (1981)
13	Basalt	30.4±1.0[(a)]	05.58.00	36.21.49	Sial et al. (1981)
14	Basalt	7.4±0.4[(b)]	05.54.38	36.27.14	Knesel et al. (2011)
14	Basalt	7.8±0.3[(b)]	05.54.38	36.27.14	Knesel et al. (2011)
15	Basalt	29.7±0.6[(b)]	05.58.00	36.21.45	Araújo et al. (2001)
16	Basalt	29.3±2[(a)]	05.58.00	36.21.45	Sial et al. (1981)
16	Basalt	29.6±3[(a)]	05.58.00	36.21.45	Sial et al. (1981)
Offshore					
19	Basalt	19.0±6.0[(a)]	05.18.42	37.28.04	Mizusaki and Saracchini (1991), apud Mizusaki et al. (2002)
20	Basalt	28.0±7.0[(a)]	04.54.54	36.17.59	Mizusaki and Saracchini (1991), apud Mizusaki et al. (2002)
21	Basalt	29.0±1.8[(a)]	04.55.00	36.15.00	Fodor and McKee (1986)
21	Basalt	36.3±2.0[(a)]	04.55.00	36.15.00	Fodor and McKee (1986)
22	Basalt	42.0±3.0[(a)]	04.55.36	36.28.04	Mizusaki (1989)
23	Basalt	37.0±7.0[(a)]	04.55.39	36.14.32	Mizusaki and Saracchini (1991), apud Mizusaki et al. (2002)
23	Basalt	37.0±9.0[(a)]	04.55.39	36.14.32	Mizusaki and Saracchini (1991), apud Mizusaki et al. (2002)
23	Basalt	47.0±1.0[(a)]	04.55.39	36.14.32	Mizusaki and Saracchini (1991), apud Mizusaki et al. (2002)
23	Diabase	44.0±4.0[(a)]	04.55.39	36.14.32	Mizusaki and Saracchini (1991), apud Mizusaki et al. (2002)

24	Basalt	44.6 ±6.6[a]	04.55.40	36.14.33	Mizusaki (1989)
25	Basalt	33.0±1.0[a]	04.56.41	36.09.57	Mizusaki (1989)
25	Basalt	32.0±1.0[a]	04.56.41	36.09.57	Mizusaki and Saracchini (1991), apud Mizusaki et al. (2002)

[a] K-Ar age, [b] $^{40}Ar/^{39}Ar$ age.

Table 2

Table 2 - Stress tensors from fault-slip data. site, outcrop location or outcrop groups shown in Figures 4 and 6; N° = number of measurements used to compute the stress tensors; Phase = relative age of stress tensor; Unit age = age discussed in section 2.1 (Tur = Turonian; Cam = Campanian; Alb = Albian; Cen = Cenomanian; σ1, σ2, and σ3 = dip direction and plunge of striaes; R = relative ratio between principal stress axes; stress regime: SS = strike-slip; N = normal; R = reverse.

Site	N°	Phase	Unit age	σ1	σ2	σ3	R	Stress regime
1	4	1	Tur-Cam	340/15	175/75	071/04	0.4669	SS
2	18	2	Miocene	094/01	197/84	004/06	0.0616	SS
3	15	1	Tur-Cam	354/05	107/78	263/11	0.3556	SS
	28	2		270/05	169/63	003/26	0.1258	SS
4	28	1	Alb-Cen	177/06	297/78	086/10	0.573	SS
	13	2		072/06	185/74	341/15	0.7847	SS
5	66	1	Alb-Cen	211/77	009/12	100	0.2948	N
	40	2		253/03	344/16	154/74	0.3567	R
6	39	1	Tur-Cam	008/04	098/04	232/85	0.794	R
	16	2		276/12	010/18	154/68	0.0481	R
7	11	1	Tur-Cam	356/00	266/02	086/88	0.3711	R
8	132	1	Tur-Cam	351/07	245/66	084/23	0.6267	SS
9	14	1	Alb-Cen	214/10	083/75	306/11	0.727	SS
	26	2		096/09	198/54	360/34	0.4333	SS
10	190	1	Tur-Cam	350/03	255/59	082/31	0.7876	SS
	8	2		070/17	263/72	161/04	0.6993	SS
11	26	2	Albian-Cen	267/07	171/43	004/46	0.7049	SS
12	74	2	Late Quaternary	273/08	129/81	004/06	0.3178	SS
13	53	2	Late Quaternary	090/04	224/84	360/04	0.5198	SS
14	64	1	Miocene	006/05	240/81	096/07	0.2498	SS
15	15	1	Miocene	357/06	158/84	267/02	0.5176	SS
16	39	2	Late Quaternary	103/00	193/02	007/88	0.9928	R
17	7	1	Tur-Cam	001/02	220/87	091/02	0.4459	SS
18	40	1	Miocene	021/81	186/09	276/02	0.8234	N
19	25	1	Tur-Cam	357/02	184/88	087/00	0.4212	SS
20	34	1	Alb-Cen	008/12	135/72	275/14	0.3508	SS
	22	2		269/02	027/85	179/04	0.4087	SS
21	21	1	Tur-Cam	343/06	074/06	212/82	0.5985	R
	11	2		079/11	342/24	192/63	0.2025	R
22	37	1	Alb-Cen	007/00	099/78	277/12	0.5421	SS
	21	2		279/00	009/76	189/14	0.4664	SS
23	39	1	Tur-Cam	012/09	281/05	162/79	0.1617	R
	54	2		257/02	347/04	139/86	0.7380	R
24	27	1	Alb-Cen	019/03	236/87	109/02	0.3313	SS
25	182	1	Tur-Cam	182/00	272/00	041/90	0.9810	R

	57	2		095/01	256/89	005/00	0.6945	SS
26	75	1	Tur-Cam	182/00	288/89	092/01	0.1336	SS
	37	2		107/03	274/87	017/01	0.8908	SS
27	17	2	Miocene	270/12	119/77	001/06	0.7584	SS
28	18	2	Miocene	060/00	327/87	150/03	0.1577	SS
29	51	1	Tur-Cam	167/03	077/08	274/81	0.2185	R
	14	2		039/88	240/02	150/01	0.0906	N
30	37	1	Albian-Cen	004/04	204/86	094/01	0.4825	SS
	56	2		277/17	109/72	008/03	0.9723	SS